MSC-01274

NATIONAL AERONAUTICS AND SPACE ADMINISTRATION

NASA PROGRAM APOLLO WORKING PAPER

THERMAL PERFORMANCE AND RADIO-FREQUENCY TRANSMISSIVITY OF CANDIDATE ABLATION MATERIALS FOR S-BAND ANTENNA WINDOW APPLICATION ON MANNED SPACECRAFT

(NASA-TM-X-68325) THERMAL PERFORMANCE AND RADIO-FREQUENCY TRANSMISSIVITY OF CANDIDATE ABLATION MATERIALS FOR S-BAND ANTENNA WINDOW APPLICATION ON MANNED D.J. Tillian, et al (NASA) Jun. 1970 78 p CSCL 09E G3/09

N72-22220

Unclas 24625

MANNED SPACECRAFT CENTER
HOUSTON, TEXAS
June 1970

MSC-01274

NASA PROGRAM APOLLO WORKING PAPER

THERMAL PERFORMANCE AND RADIO-FREQUENCY TRANSMISSIVITY OF CANDIDATE ABLATION MATERIALS FOR S-BAND ANTENNA WINDOW APPLICATION ON MANNED SPACECRAFT

PREPARED BY

Donald J. Tillian

Donald J. Tillian
Structures and Mechanics Division

H. Dean Cubley

H. Dean Cubley
Telecommunications Systems Division

AUTHORIZED FOR DISTRIBUTION

Warren Gillespie, Jr.

for Maxime A. Faget
Director of Engineering and Development

NATIONAL AERONAUTICS AND SPACE ADMINISTRATION
MANNED SPACECRAFT CENTER
HOUSTON, TEXAS
June 1970

PRECEDING PAGE BLANK NOT FILMED

CONTENTS

FIGURES

THERMAL PERFORMANCE AND RADIO-FREQUENCY TRANSMISSIVITY OF CANDIDATE ABLATION MATERIALS FOR S-BAND ANTENNA WINDOW APPLICATION ON MANNED SPACECRAFT

By Donald J. Tillian and H. Dean Cubley

SUMMARY

A test program was conducted in the MSC 1.5 MW arc-heated facili to evaluate the thermal performance of ablation materials having pote tial application as radio frequency (RF) windows. These tests were conducted in support of Contract NAS 9-8334 with Litton Industries fo the improvement of omnidirectional antenna operating characteristics during atmospheric reentry. Since a full scale model of the Apollo Command Service Module (CSM) was available for antenna tests, this mockup was used as a basis for the tests. Test models were subjected to heating conditions simulating the nominal lunar return trajectory (AS-501) and the design trajectories, high heat load (HL-1) and high heating rate (HR-1). RF measurements were made before and after the arc jet tests to measure attenuation effects due to the thermal degra- dation of the materials under consideration. The test program demon- strated that additional development is required in materials technolo to achieve an ablative system with both good RF transmission characte istics and thermal-structural integrity.

INTRODUCTION

The Apollo Command Module S-band omnidirectional antenna system consists of an array of four cavity-backed helical antennas which pr vide communications to distances of 2500 nautical miles or for any p iod in the mission when the high gain antenna cannot be used. These tennas spaced at 90° positions from each other are mounted on the ma imum radius of the spacecraft toroid section, as shown in figure 1. Two of the S-band antennas located on the leeward side of the space- craft are directly exposed to reentry heating conditions. The other two antennas located on the windward side of the spacecraft are mount under 0.7-inch thick window covers of Avcoat 5026-39M ablation materi During reentry from a nominal lunar return mission, the Avcoat ablato material windows form a char layer approximately 0.3-inch thick which

results in RF transmission attenuation on the order of 30 dB. An S-band antenna improvement program was undertaken through Contract NAS 9-8334 with the Amecon Division of the Litton Industries to provide better communication coverage between spacecraft-to-ground installations.

A ground test program was implemented in the MSC 1.5 MW arc-heated facility to evaluate the thermal performance of candidate ablation materials having good RF transmission characteristics. During this test program, 18 ablation models were subjected to heating rate and heat load conditions experienced during atmospheric reentry from a lunar mission. Radio frequency transmission loss tests were conducted in the MSC antenna range facilities before and after the arc jet tests. The arc jet and RF transmission test results are presented in this report.

TEST MODELS

The materials evaluated during this test program were Avcoat X-9010 with a density of 112 lb/ft^3, Avcoat 480-1B with a density of 17 lb/ft^3, and GE 1004AP with a density of 35 lb/ft^3. The Avcoat materials were proprietary products developed by the Avco Space Systems Division. The GE 1004AP material was developed by the General Electric Missiles and Space Division. The ablation materials were machined as 2-inch diameter cylinders which were mounted in a 4-inch diameter blunt hemisphere shroud of the Apollo ablator, Avcoat 5026-39 HCG. The antenna window ablation materials were closed out by a fiberglas edge member, and 0.50-inch thick phenolic linen was used as the back-up structure. A chromel-alumel thermocouple was mounted to a 0.062-inch thick stainless steel (type 301) plate which was bonded with RTV 560 to the ablative antenna window materials. The test models were designed to simulate the materials and close out members in the area of the existing Apollo S-band antenna window covers. The test model configuration is shown in figure 2. The ablative models were fabricated by the Amecon organization, and final assembly was completed by personnel of the MSC 1.5 MW arc-heated facility. Test models of Avcoat 5026-39 HCG ablation materials were also fabricated for testing as the reference Apollo thermal protection system.

TEST APPARATUS AND CONDITIONS

Arc Jet Facility Test Apparatus

The test program was conducted in the 1.5 MW arc-heated tunnel at the NASA Manned Spacecraft Center. The tests were conducted with the 6-inch diameter conical nozzle of the 1.0 MW segmented constricted arc heater described in reference 1. Figure 3 shows the arc heater and associated tunnel system of the MSC 1.5 MW arc-heated facility.

Test Conditions

The predicted cold wall heating rate for a nominal lunar return trajectory (501) is shown in figure 4. The step heating pulse conditions selected to simulate the trajectory heating conditions for the nominal lunar return trajectory (501) are also shown in figure 4. The step heating pulse conditions for the design trajectories, HL-1 and HR-1, and the 501 simulation are tabulated in table I.

The heat transfer rates were measured by a Gardon gauge type sensor which was mounted in a graphite shroud having the same configuration as the test model. Heat transfer rates are obtained from a measurement of the temperature differential between the center and periphery of the thin constantan sensor element. The heat transfer rate can be calculated by the following equation:

$$\dot{q} = \frac{4\ell K \Delta T}{R^2}$$

where K = thermal conductivity of constantan (Btu/ft-°F-sec), $\dot{q}$ = incident heat transfer rate (Btu/ft^2-sec), R = radius of the constantan disc (ft), ΔT = temperature differential between center and periphery of the constantan disc (°F), and ℓ = thickness (ft) of constantan disc.

These instruments are normally calibrated by radiant energy sources in terms of millivolt output versus heat transfer rate.

The energy balance technique was applied in determining the mean enthalpy level of the arc-heated stream during the model tests. This technique requires the measurement of the power into the arc heater, the cooling water flow rates, water temperature rise through the arc heater, and total gas flow rate. This process can be described by the equation:

$$H_t = \frac{.948\ VI - \dot{m}_w C_{p_w} \Delta T_w}{\dot{m}g}$$

where C_{p_w} = specific heat of water (Btu/lb-°F), H_t = average total enthalpy of gas stream (Btu/lb), I = current (amperage), $\dot{m}g$ = gas flow rate (lb/sec), $\dot{m}_w$ = water flow rate (lb/sec), V = voltage (volts), ΔT_w = water temperature rise (°F).

Surface temperatures of the models were measured by an automatic optical pyrometer operating at a wavelength of 0.65 microns. These data are presented in table I with the model test condition data. Impact pressure measurements taken at the centerline of the arc-heated stream with a pitot pressure probe are presented in table I.

TEST PROCEDURE

Arc Jet Test Procedure

RF transmission tests of the model were conducted by Telecommunication Systems Division (TCSD) personnel prior to the arc jet tests. Upon completion of the RF tests, weight and dimensional measurements were taken of each model. The models were then installed on the insertion arms in the 1.5 MW arc-heated tunnel. The test procedure followed during the trajectory simulation tests was to start the arc heater, establish the desired test conditions by insertion of the heat transfer rate calibration model and pitot probe, and then insert the test model at the required time sequence. Upon completion of the arc jet tests, post test weights, dimensional measurements, and photographs were taken of each test model. RF transmission measurements were taken of all the test models upon completion of the arc jet tests. The models were cross-sectioned to determine the char thermal degradation depths upon completion of the RF tests.

RF Transmission Test Configuration

RF transmission attenuation tests were conducted on the 15 window materials samples described in the preceding section. These tests were conducted by the TCSD in the MSC antenna range test facilities. The purpose of these RF transmission attenuation tests was to evaluate the performance of Avcoat X-9010, Avcoat 480-1B, and GE 1004AP material as possible CSM omnidirectional antenna covering material. The suitable performance of one or more of these materials would allow a considerable improvement in communications during future space missions.

The procedure followed in the test of these samples consisted of performing RF transmission attenuation and voltage standing wave ratio (VSWR) tests before and after the exposure of these samples to the various thermal environments. In order to make these tests as realistic as possible, each test sample was mounted over an actual CSM antenna mounted in a partial mockup of the command module. This test configuration provided a sufficiently realistic environment for the test such that the antenna patterns were almost identical to those on an actual spacecraft. Using this test configuration, a complete set of principal plane antenna patterns was taken at the test frequency of 2287.5 MHz prior to the exposure of the samples to the thermal environment. At the

end of the recording of antenna patterns for each sample, a VSWR reading was taken for each sample while the sample was still mounted in the test mockup. At the completion of this test, a reference set of patterns was taken for an antenna mounted in the same test configuration but with the covering material over the antenna removed. Following the completion of the thermal tests on the samples, the entire test sequence was repeated on all but three of the test samples. These three test samples were composed of Avcoat X-9010 material which distorted during thermal tests to the point where pattern and VSWR tests would have been meaningless.

TEST RESULTS AND DISCUSSION

Arc Jet Test Results

The results from the arc jet tests are summarized in tables I and II. Table I is a tabulation of the environmental conditions; table II contains the model ablation data. Appearance of the materials before and after testing is shown in figures 5 to 26. A convenient parameter for evaluating the relative ablative efficiency of materials can be evaluated from the experimental data in the following manner:

$$Q_{cw}^* = \frac{\dot{q}_{cw}}{\dot{m}}$$

where Q_{cw}^* is defined as the cold wall heat of ablation (Btu/lb), $\dot{q}_{cw}$ is the cold wall heat transfer rate (Btu/ft^2-sec), and $\dot{m}$ is the mass loss rate (lb/ft^2-sec).

The thermal effectiveness of the three candidate S-band window materials for two steady-state heating conditions is presented in figure 27. The thermal effectiveness of all three materials increased with increased heat transfer rate conditions. The best thermal performance was exhibited by the GE 1004AP and Avcoat 480-1B low density ablators. Similar performance can also be observed in figure 28 in which the maximum backface temperature for the materials is presented for three test conditions. The backface temperature-time histories for all of the test models are presented in figures 29 to 43. Over the range of test conditions, the GE 1004AP and Avcoat 480-1B materials, which were elastomers, formed comparatively strong and symmetrical char layers with the Apollo ablator shrouds.

Considerable difficulty was experienced in testing the Avcoat X-9010, which was a celcon quartz material. Considerable thermal expansion of the Avcoat X-9010 material occurred during the arc jet tests,

which resulted in several model failures. This problem may result from the quartz fiber layout in the celcon quartz material. It is possible that significant improvement could be obtained by a random quartz fiber orientation.

Satisfactory thermal performance was demonstrated by all of the materials for the high heating rate/short test time HR-1 simulation. The performance of all of the materials with the present 0.7-inch thick ablator requirement appears marginal for the high heat load (HL-1) trajectory as evidenced by the high backface temperatures in figures 30, 38, and 41. Further investigations and analyses would have to be conducted with a thermal model of the S-band antenna assembly to fully define this problem.

Based on the temperature measurements and model ablation performance, satisfactory thermal performance was exhibited by all three materials for the nominal lunar return trajectory (501). However, improvement in the Avcoat X-9010 material is considered desirable, based on the extensive warpage observed on the test models and failures at the higher heat load test conditions.

RF Test Results

The results of all of the RF tests were recorded either in the form of antenna patterns on polar plots or VSWR readings. The RF test data was reduced to the form of graphs as shown in figures 44 through 59.

RF tests before thermal testing.- Figures 44 through 46 show the relative gain of a CSM omniantenna versus the angle from the antenna boresight. These graphs show gain for each of the three materials under test relative to the same CSM antenna with the covering material revoved. Figure 44 shows that the gain of the CSM omniantenna covered with GE 1004AP material is greater near the antenna boresight angle than for the uncovered antenna. The reason for this effect is that the covering material exhibits a lens effect and tends to focus the pattern of the omniantenna as compared to the gain of the uncovered antenna. This effect is also evident in figure 45 and figure 46 for the Avcoat X-9010 material and the Avcoat 480-1B material, respectively. The results of this focus effect can also be seen for the angles near the plane of the antenna for all three samples. In the region near 90° from boresight, the gain of the antenna under the sample is considerable less than that for the uncovered antenna. The results of the VSWR tests on the three different materials prior to the thermal tests indicated little if any degradation in antenna performance as a result of the covering material. In summary, the test results prior to thermal testing indicated that any one of the three candidate materials would be equally acceptable from an RF standpoint.

<u>RF tests after thermal testing</u>.- Figures 47 through 59 show the results of the RF testing after the test samples were subjected to the various thermal environments described in the other portions of this report. The gains given in these figures are also with respect to the CSM omnipattern without a covering material.

Upon examination of the data displayed in figures 47 through 51 for the GE 1004AP material, one can see that a considerable deterioration in performance resulted from exposure to the thermal environment. In general, the RF insertion loss of the material is in the range of 15 to 20 dB for all of the GE 1004AP test samples.

As mentioned previously, there was a problem with the Avcoat X-9010 material because of mechanical distortion during the thermal tests. Because of this distortion, only two of the five test samples were suitble for RF testing following the thermal tests. Data from the two Avcoat X-9010 test samples that did undergo RF testing following thermal exposure are displayed in figures 52 and 53 for test models 7 and 8, respectively. These figures show that the Avcoat X-9010 does in fact exhibit very favorable electrical performance following thermal exposure. The average insertion loss for both of these test samples is shown to be only 2 to 3 dB over the portion of the antenna pattern that is of major interest.

Figures 54 through 58 show the RF test data for the Avcoat 480-1B material after thermal exposure. These data indicate that the Avcoat 480-1B material performance is very similar to the GE 1004AP performance. RF transmission attenuation for the Avcoat 480-1B is consistently in the range of 15 to 20 dB.

Figure 59 shows the VSWR readings for all of the three materials by sample number following the thermal exposure. These data indicate that acceptable VSWR recordings were obtained only for the Avcoat X-9010 material. The VSWR recordings for this material were limited, however, to samples 7 and 8 because of the mechanical failure of the other samples of this material during thermal testing.

CONCLUDING REMARKS

Arc jet trajectory simulation tests were conducted on three ablators having potential application as S-band antenna window covers on the Apollo Command Module. The elastomeric materials exhibited the best thermal performance over the range of anticipated heating conditions expected on the S-band antenna windows during atmospheric reentry.

The Avcoat X-9010 was the only material which was acceptable from an RF standpoint. However, structural instabilities which occurred during the arc jet tests indicate that improvements in the Avcoat X-9010 material are necessary. The test program demonstrated that additional development is required in materials technology to achieve an ablative system with both good RF transmission characteristics and thermal-structural integrity.

REFERENCES

1. Richter, Robert, and Buhler, Rolf D.: High Enthalpy Gas Heater. NASA CR-65268, 1966.

TABLE I.- MODEL TEST CONDITIONS

Model number	Test number	Material	Simu-lation	Heat flux, Btu/ft^2-sec	Test time, sec	Heat load, Btu/ft^2	Enthalpy, Btu/lb	Pitot pressure, atm	Model surface tempera-ture, °F, ϵ = 1.0
1	514	GE 1004	501	75 0 35	50 300 100	3750 3500	7900 6400	0.0067 .0060	2890
2	515	GE 1004	HL-1	75 0 45	120 0 150	9000 6750	7900 6400	.0067 .0060	2950 2770
3	516	GE 1004		77	120	9240	7900	.0068	3020
4	517	GE 1004	HR-1	245	40	9800	11350	.0087	
5	527	GE 1004	501	75 30	50 100	3750 3000	7900 6200	.0067 .0059	3000
6	512	Avco X-9010	501	75 0 45	50 300 100	3750 4500	7900 6400	.0067 .0060	2750
7	523	Avco X-9010	HR-1	246	40	9840	11350	.0087	
8	524	Avco X-9010		76	120	9120	7900	.0067	2800
9	525	Avco X-9010	501	73 0 32	50 300 100	3650 3200	7900 6200	.0067 .0059	2880
10	526	Avco X-9010	HL-1	77 0 34	120 300 100	9240 3400	7900 6200	.0068 .0059	2790
11	513	Avco 480-1B	501	76 0 45	50 300 100	3800 4500	7900 6400	.0068 .0060	2940
12	518	Avco 480-1B	501	80 0 33	50 300 100	4000 3300	8000 6200	.0069 .0059	2950
13	519	Avco 480-1B	HL-1	75 0 33	120 300 150	9000 4950	7900 6200	.0067 .0059	2900
14	520	Avco 480-1B		78	120	9360	7900	.0068	2920

TABLE I.- MODEL TEST CONDITIONS - Concluded.

Model number	Test number	Material	Simu-lation	Heat flux, Btu/ft^2-sec	Test time, sec	Heat load, Btu/ft^2	Enthalpy, Btu/lb	Pitot pressure, atm	Model surface tempera-ture, °F, $\epsilon = 1.0$
15	521	Avco 480-1B	HR-1	244	40	9760	11350	0.0087	3280
16	509	Avco 5026-39 HCG	501	75 45	50 100	3750 4500	7900 6400	.0067 .0060	2800 —
18	511	Avco 5026-39 HCG	501	78 0 44	50 300 100	3900 4400	7900 6400	.0068 .0060	2800 —
19	522	Avco 5026-39 HCG	HR-1	238	40	9520	11300	.0084	3510

TABLE II.- MODEL ABLATION DATA

Model number	Material	Recession (in.)	Char (in.)	Char plus recession (in.)	Weight loss (g)
1	GE 1004	0.045	0.24	0.285	10.6
2	GE 1004	.170	.54	.710	23.5
3	GE 1004	.040	.29	.330	9.6
4	GE 1004	.174	.096	.270	7.6
5	GE 1004	.025	.291	.316	10.4
6	Avco X-9010	+.02	.136	.136	20.1
7	Avco X-9010	.025	.167	.182	11.3
8	Avco X-9010	+.023	.216	.216	19.8
9	Avco X-9010	.004	.244	.248	25.3
10	Avco X-9010	0	.220	.220	28.9
11	Avco 480-1B	.095	.387	.482	9.9
12	Avco 480-1B	.101	.298	.399	7.2
13	Avco 480-1B	.162	.461	.623	9.9
14	Avco 480-1B	.121	.353	.474	9.6
15	Avco 480-1B	.207	.113	.320	6.1
16	Avco 5026-39	.030	.310	.343	-
18	Avco 5026-39	.015	.360	.375	-
19	Avco 5026-39	.023	.260	.283	-

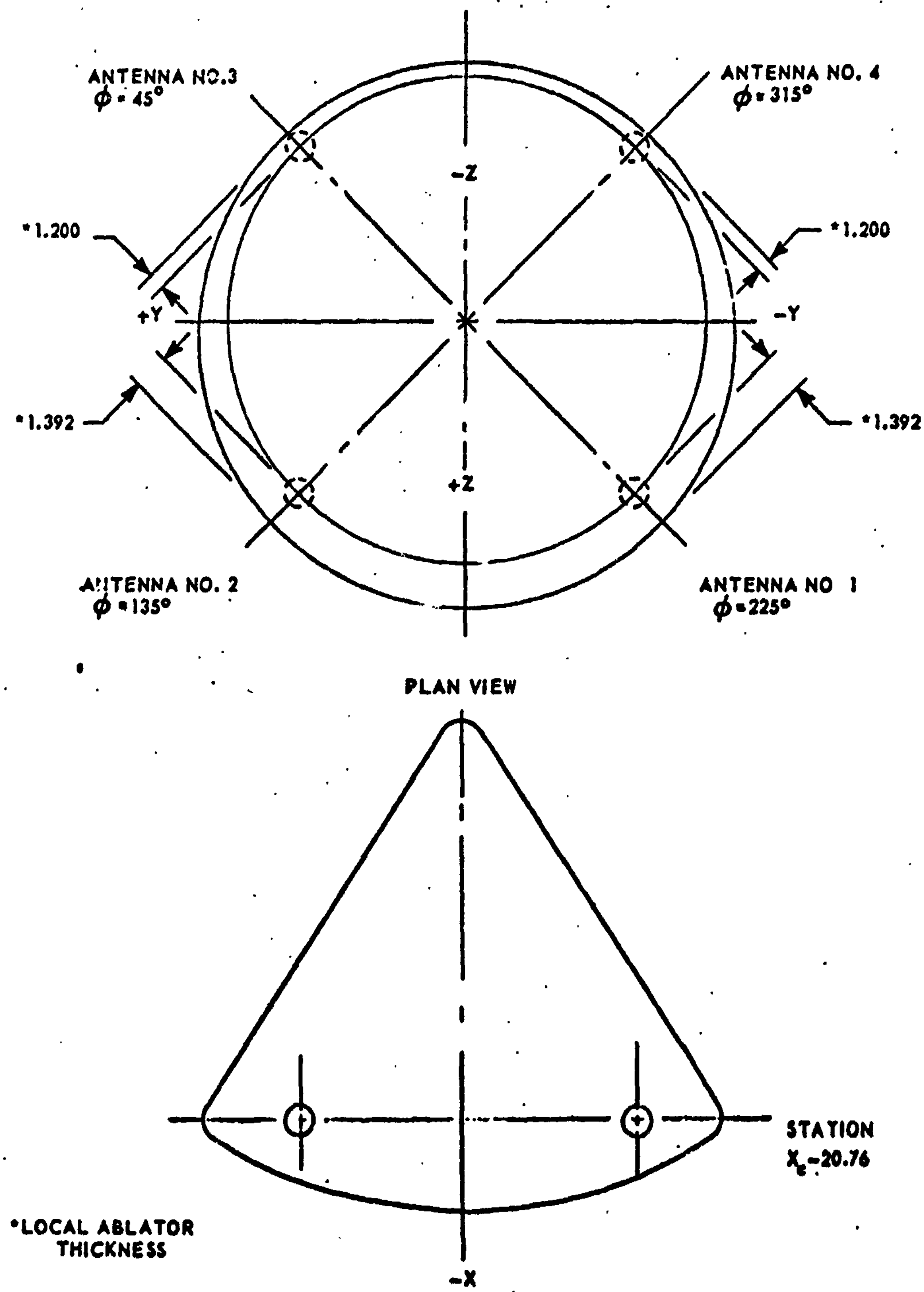

Figure 1.- S-band omniantenna locations on the Apollo Command Module.

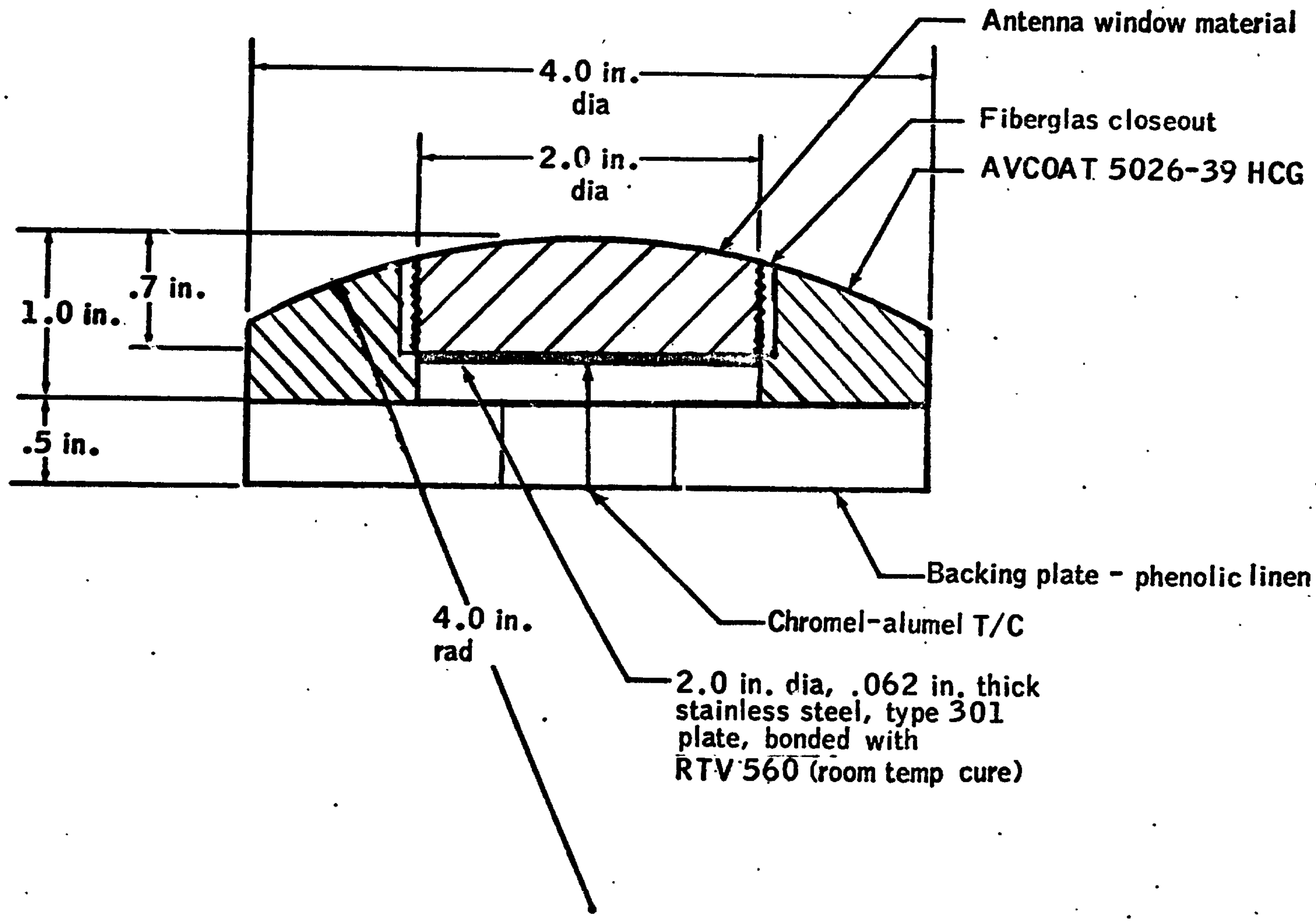

Figure 2.- S-band omnidirectional antenna window test model.

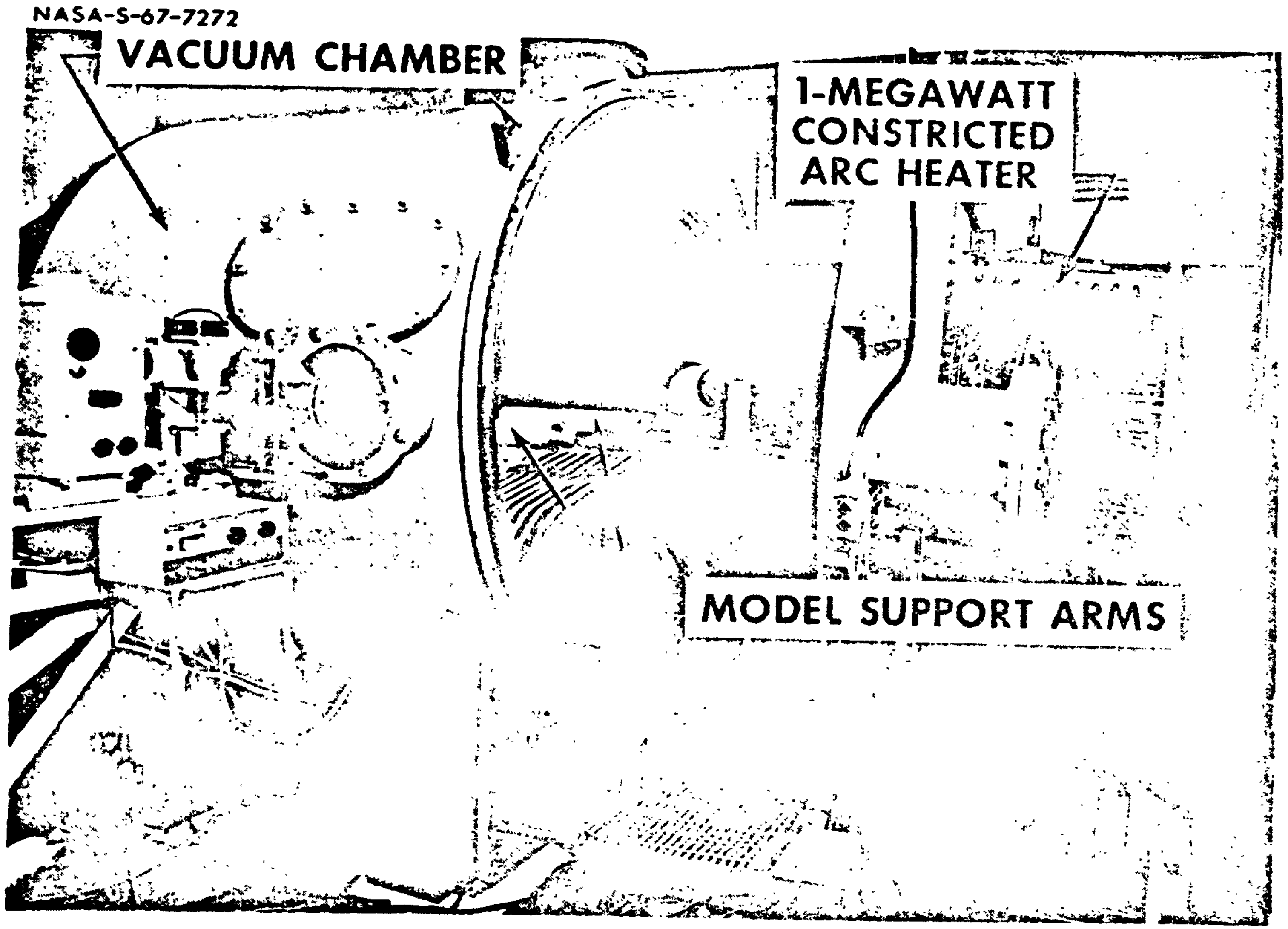

Figure 3.- NASA Manned Spacecraft Center 1.5-megawatt arc-tunnel facility.

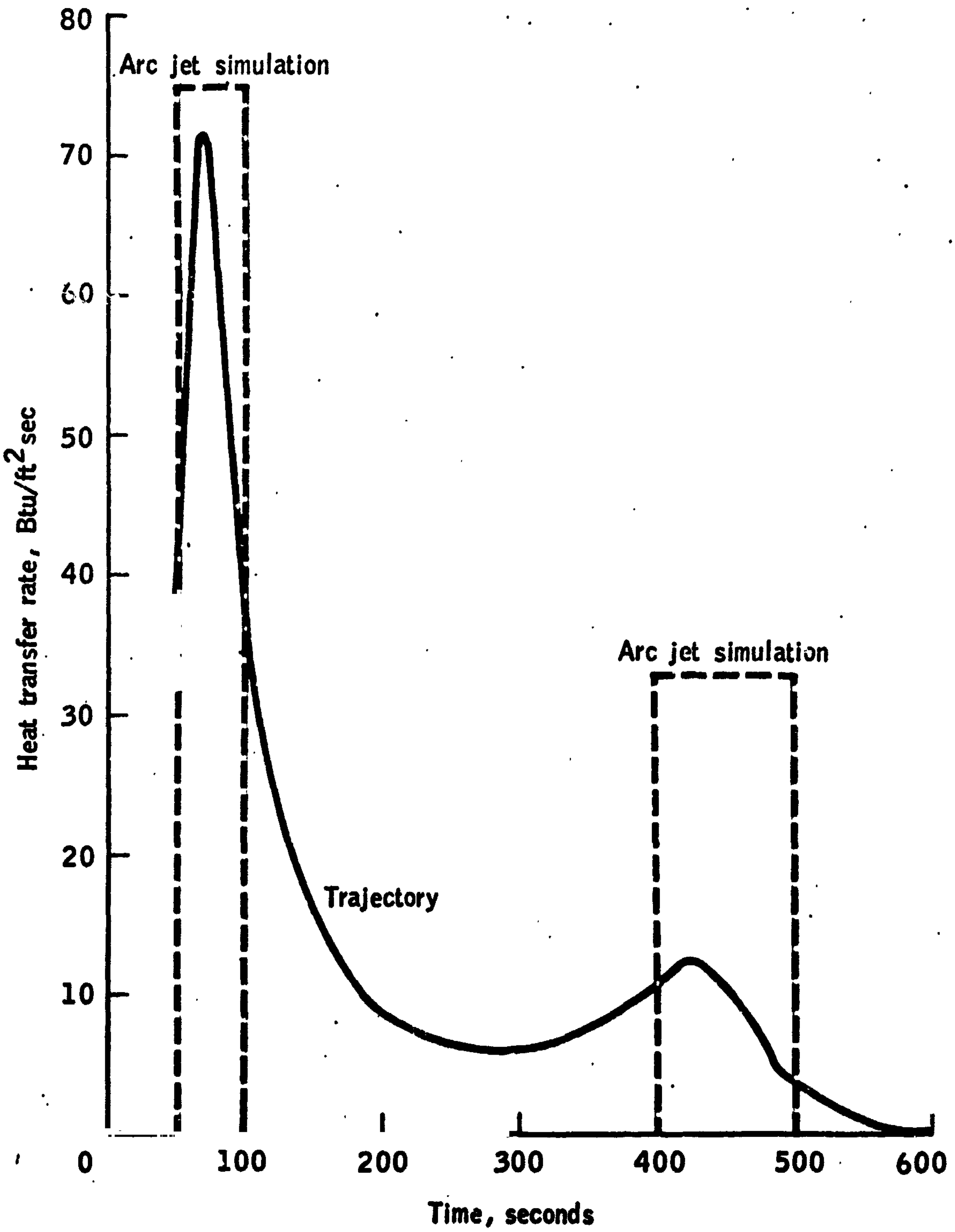

Figure 4.- Predicted cold wall heat transfer rate-time history on Apollo S-band omnidirectional antenna, θ = 45° and 135° locations based on AS-501 flight trajectory.

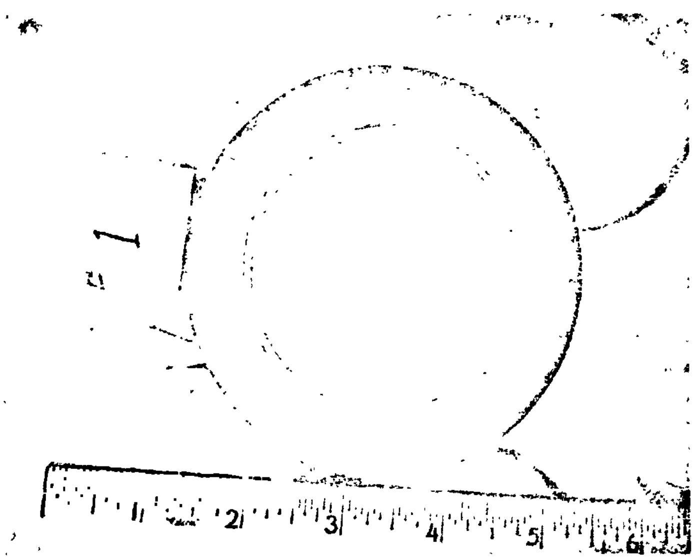

(a) Before

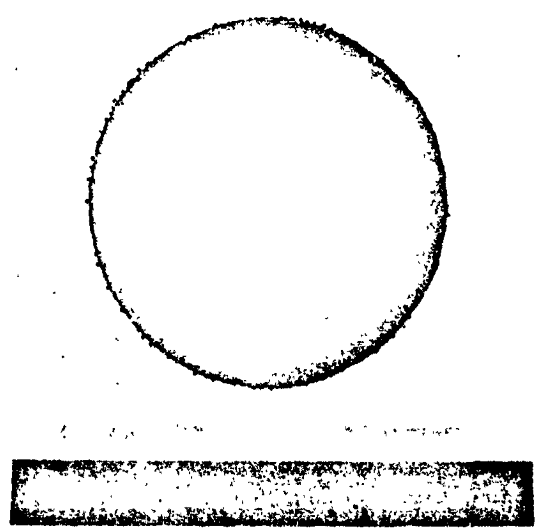

(b) After

Figure 5.- Photographs of Model 1 before and after arc jet test.

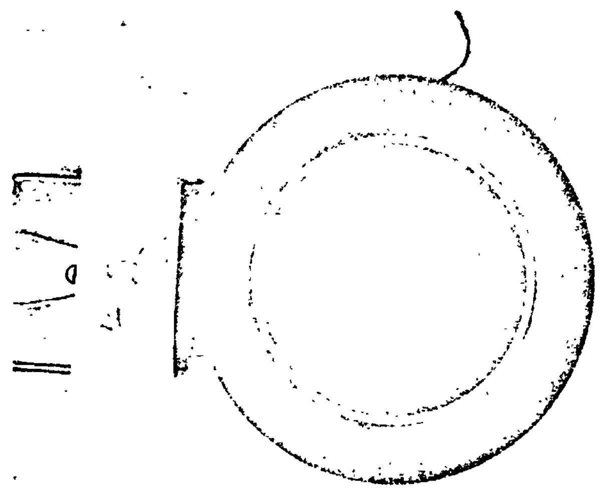

(a) Before

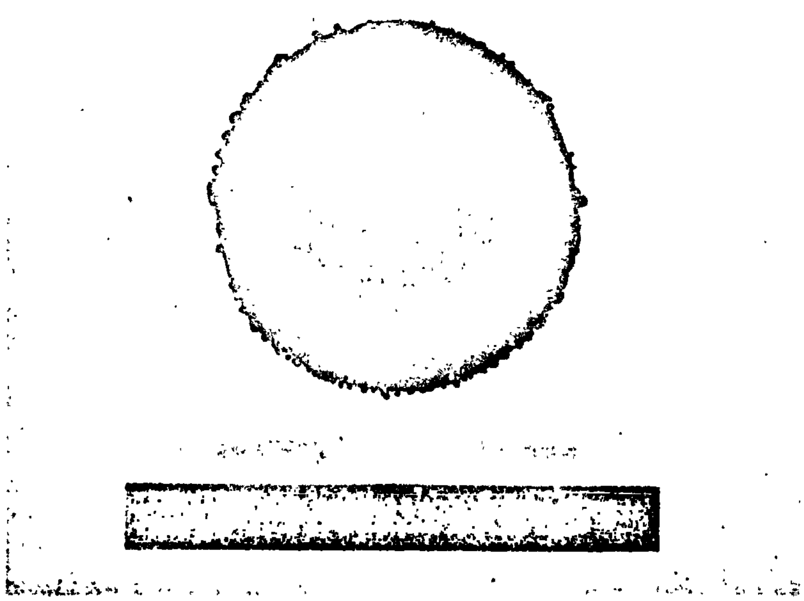

(b) After

Figure 6.- Photographs of Model 2 before and after arc jet test.

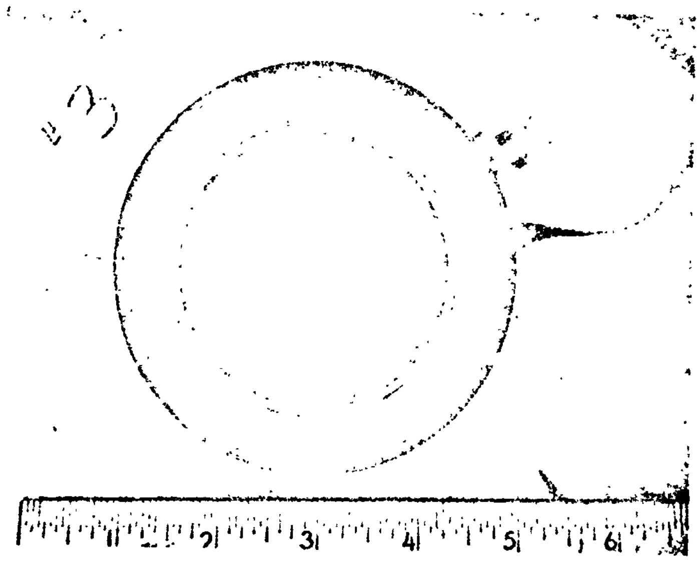

(a) Before

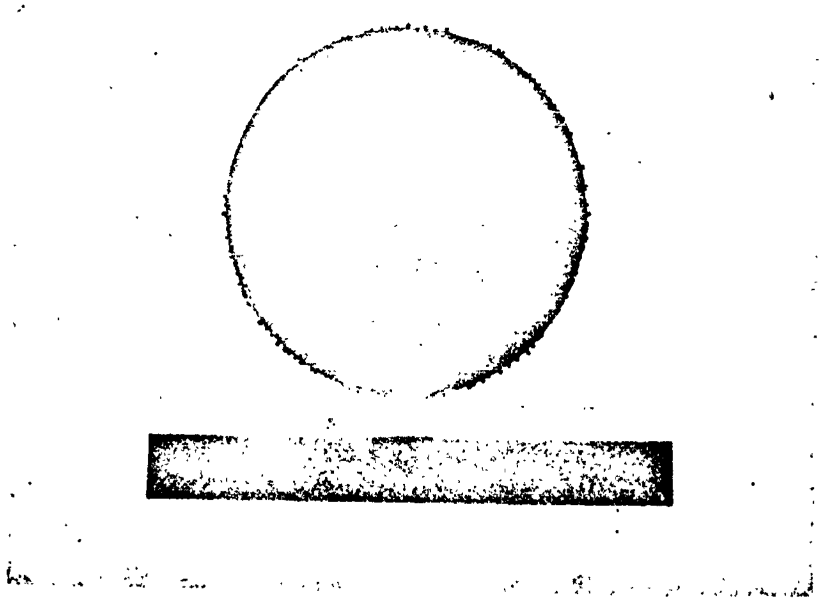

(b) After

Figure 7.- Photographs of Model 3 before and after arc jet test.

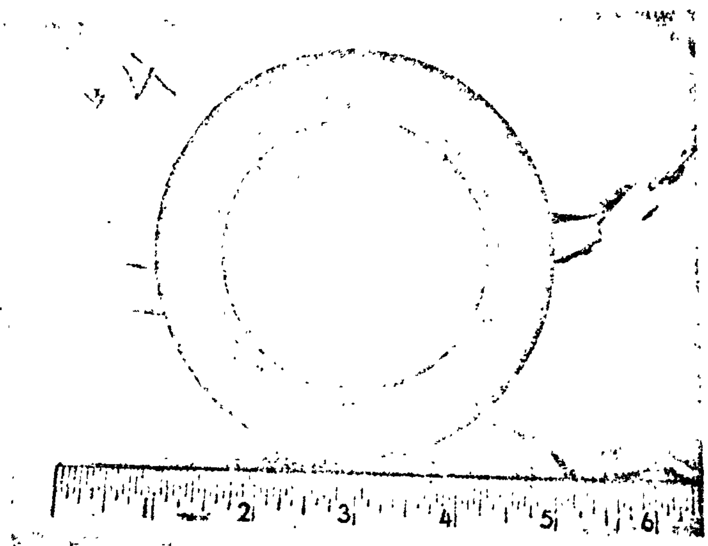

(a) Before

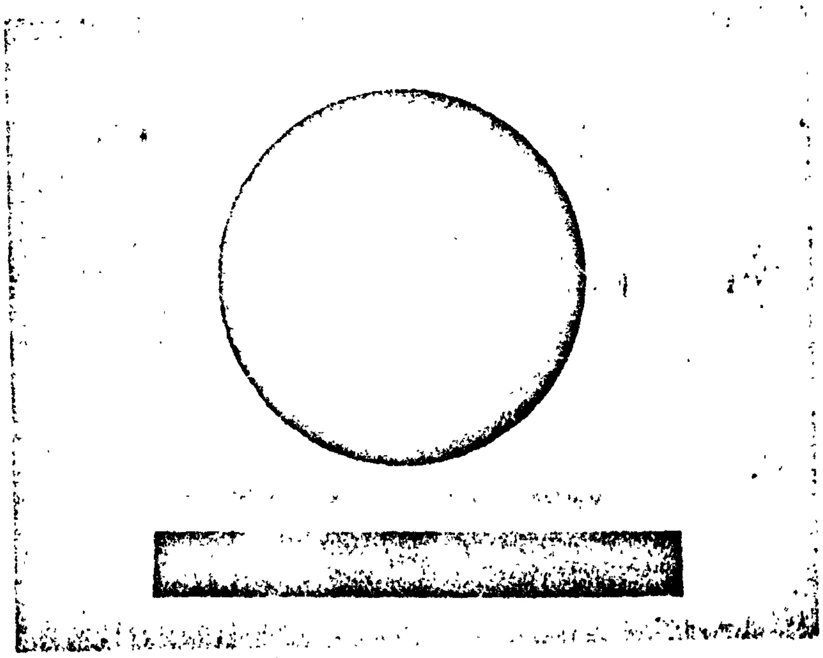

(b) After

Figure 8.- Photographs of Model 4 before and after arc jet test.

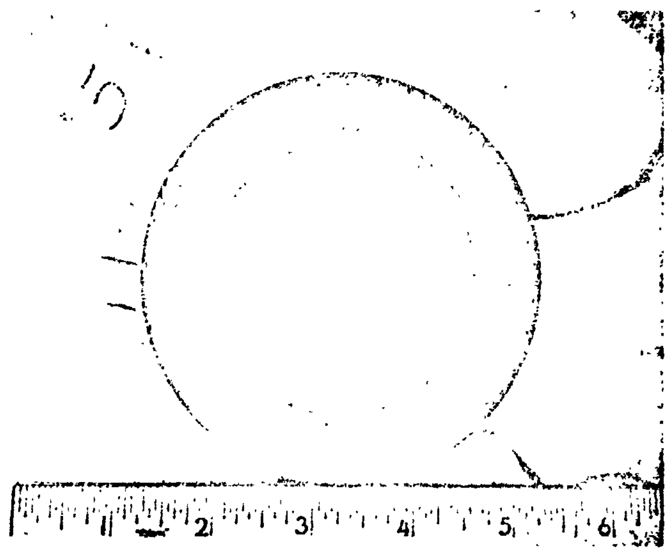

(a) Before

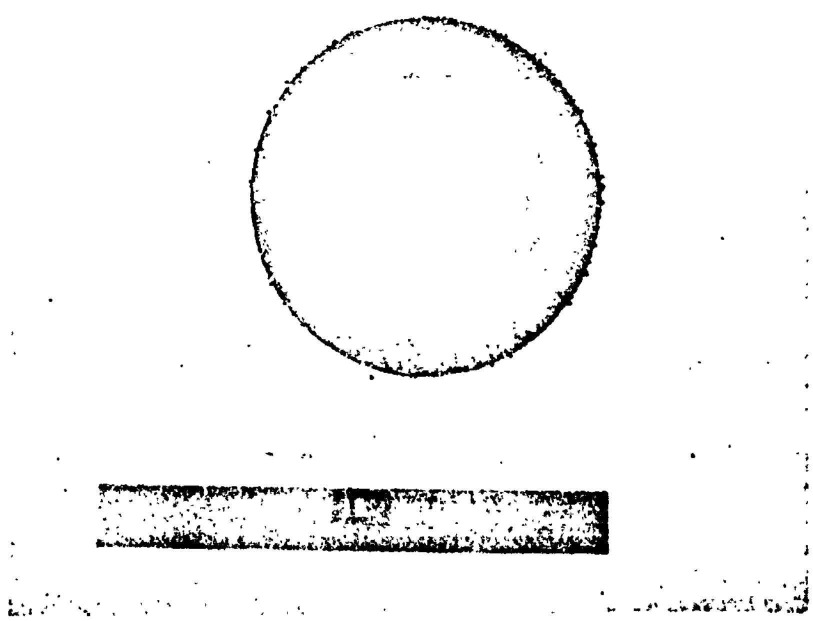

(b) After

Figure 9.- Photographs of Model 5 before and after arc jet test.

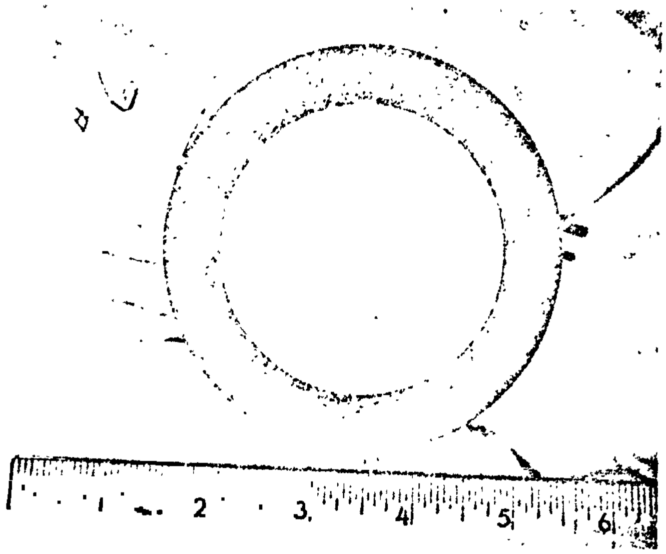

(a) Before

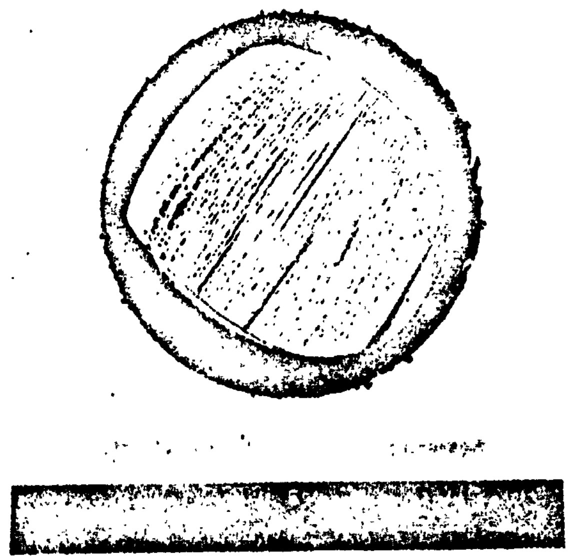

(b) After

Figure 10.- Photographs of Model 6 before and after arc jet test.

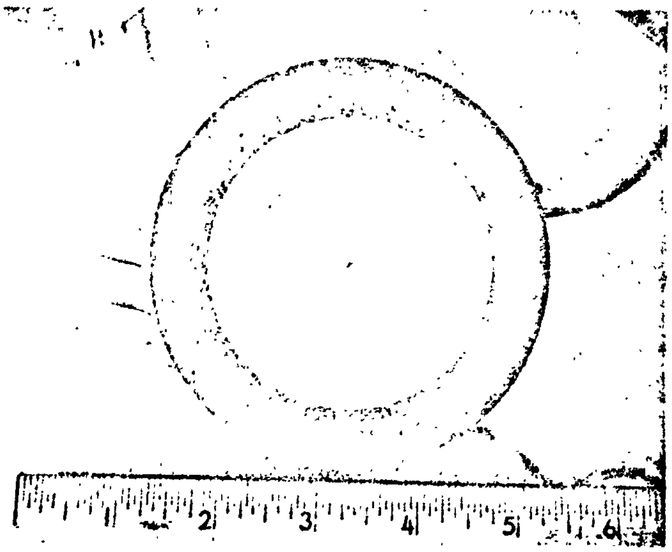

(a) Before

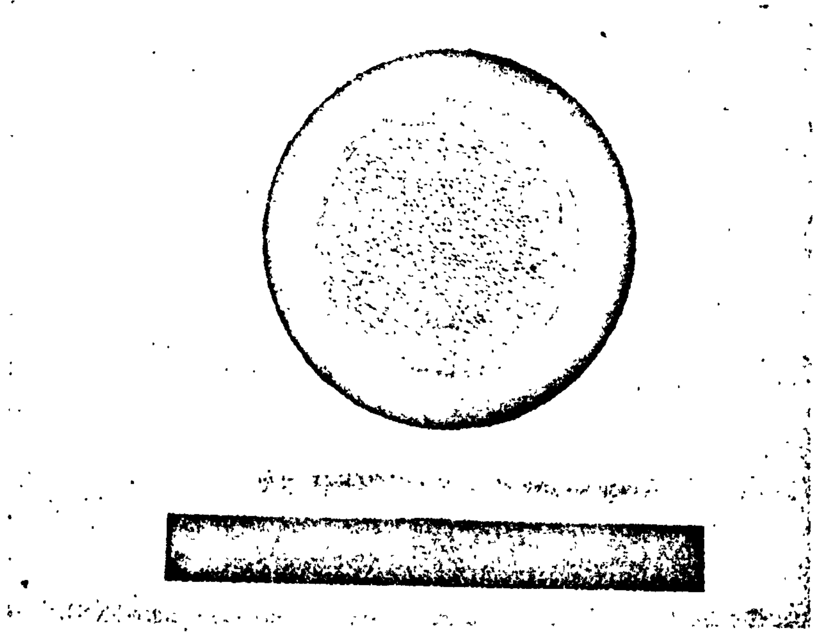

(b) After

Figure 11.- Photographs of Model 7 before and after arc jet test.

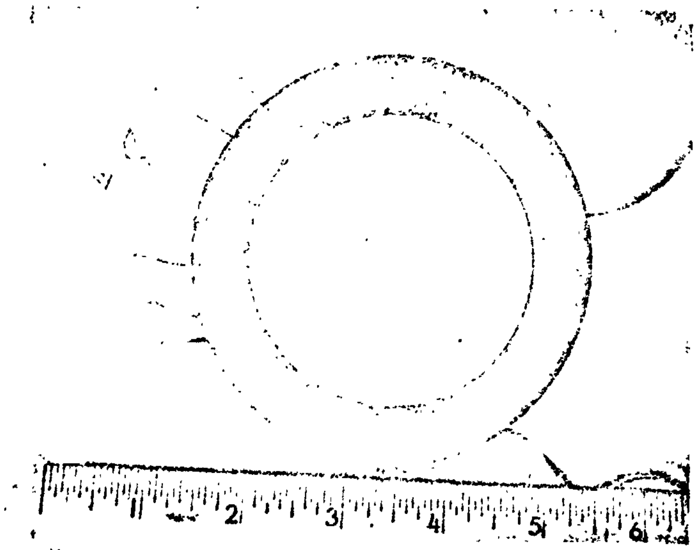

(a) Before

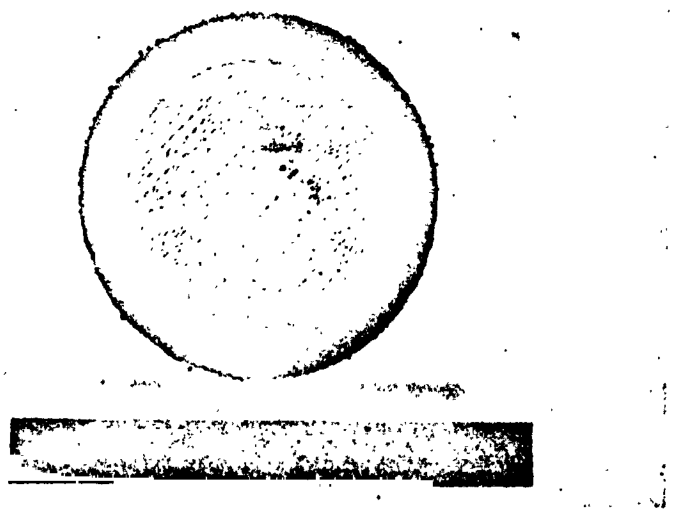

(b) After

Figure 12.- Photographs of Model 8 before and after arc jet test.

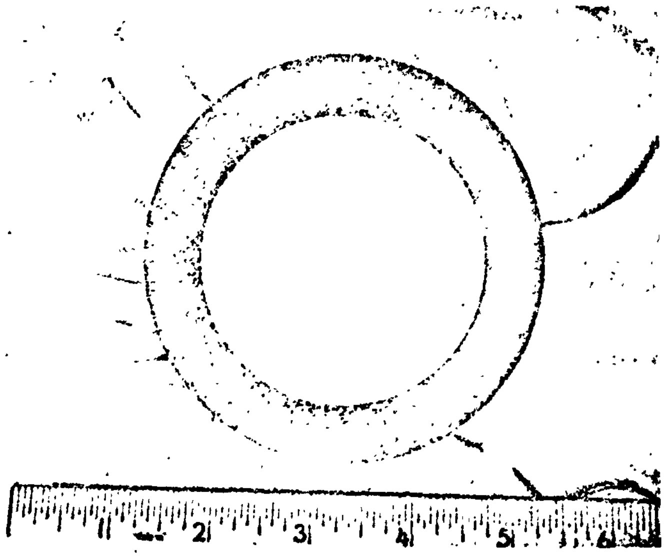

(a) Before

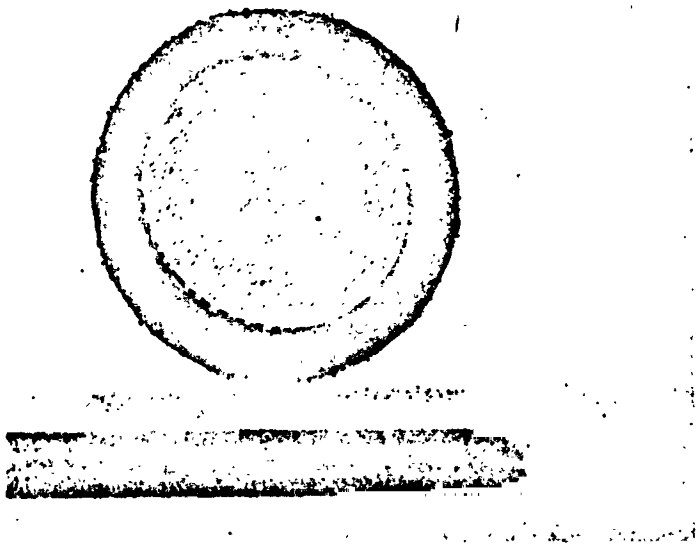

(b) After

Figure 13.- Photographs of Model 9 before and after arc jet test.

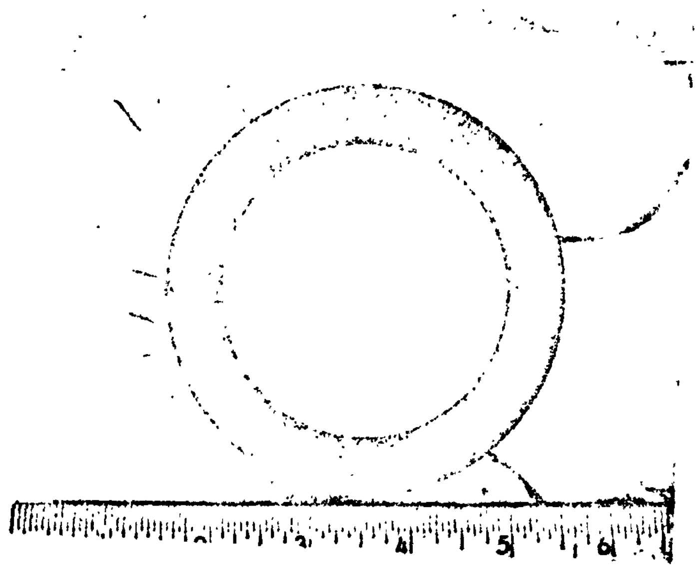

(a) Before

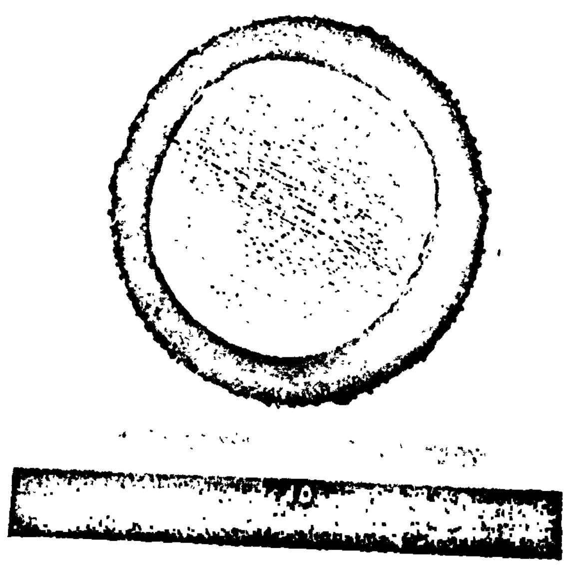

(b) After

Figure 14.- Photographs of Model 10 before and after arc jet test.

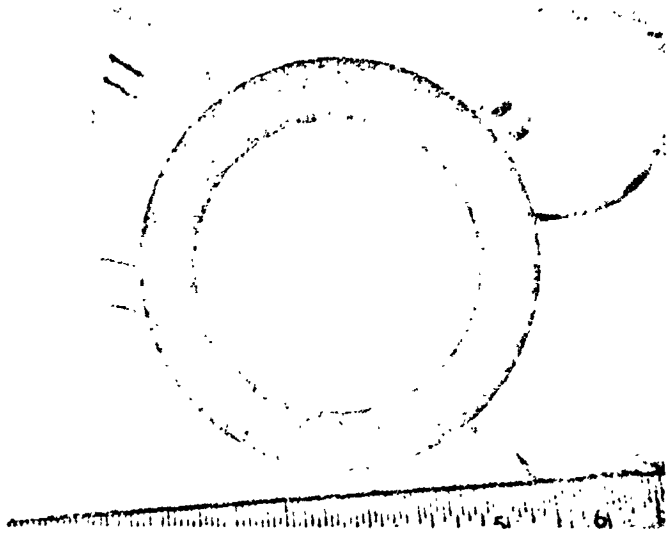

(a) Before

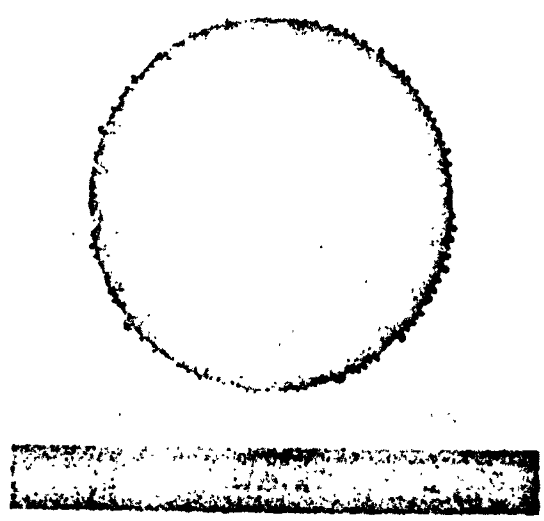

(b) After

Figure 15.- Photographs of Model 11 before and after arc jet test.

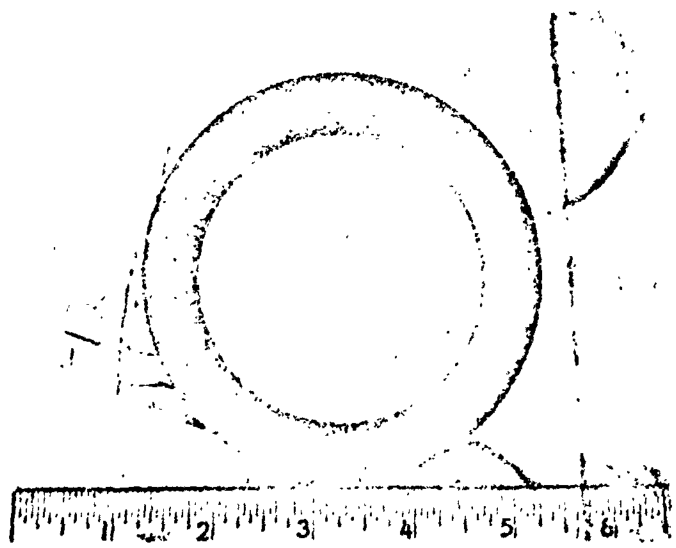

(a) Before

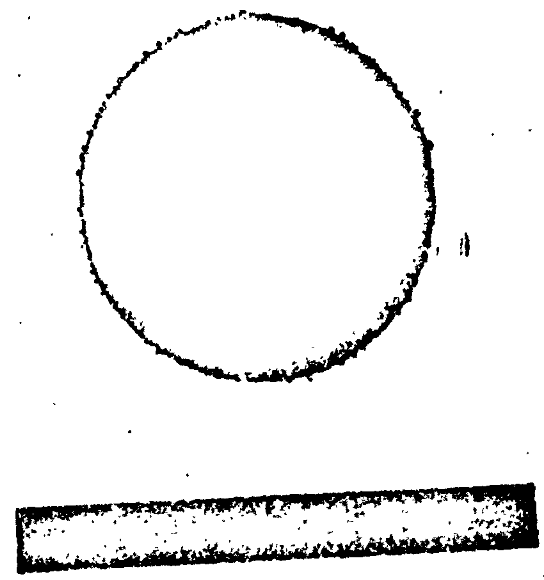

(b) After

Figure 16.- Photographs of Model 12 before and after arc jet te

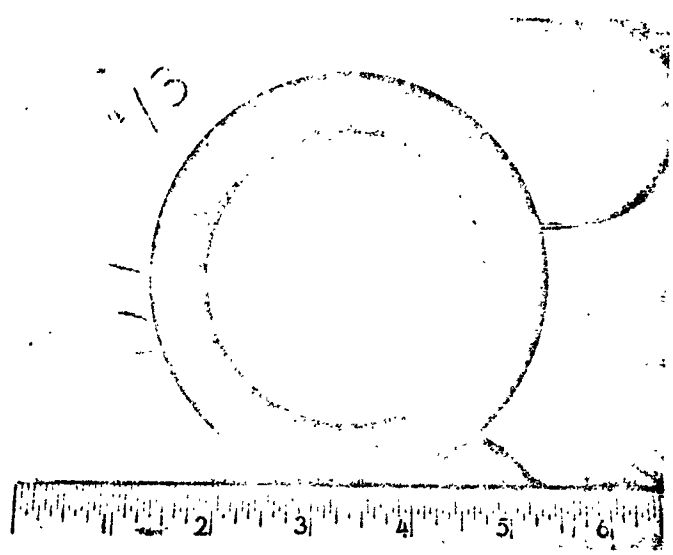

(a) Before

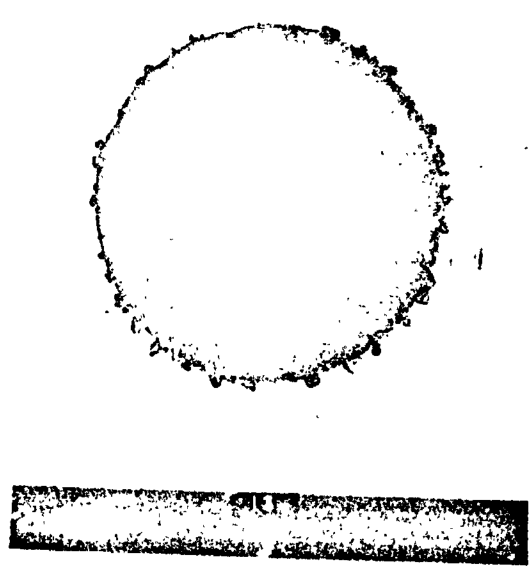

(b) After

Figure 17.- Photographs of Model 13 before and after arc jet test.

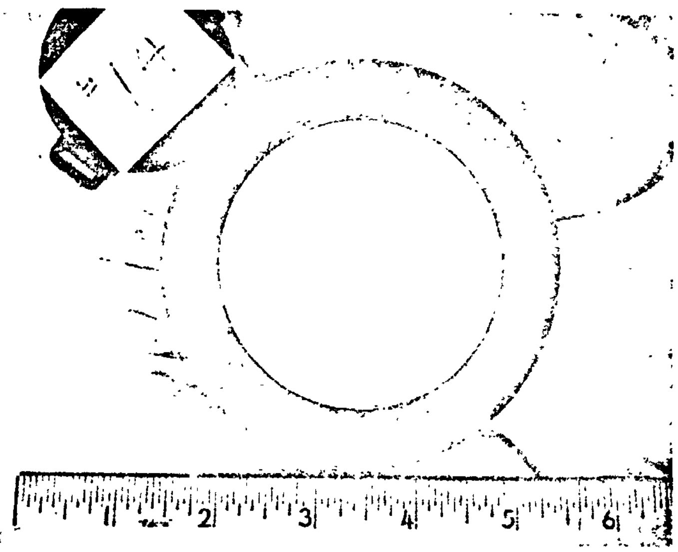

(a) Before

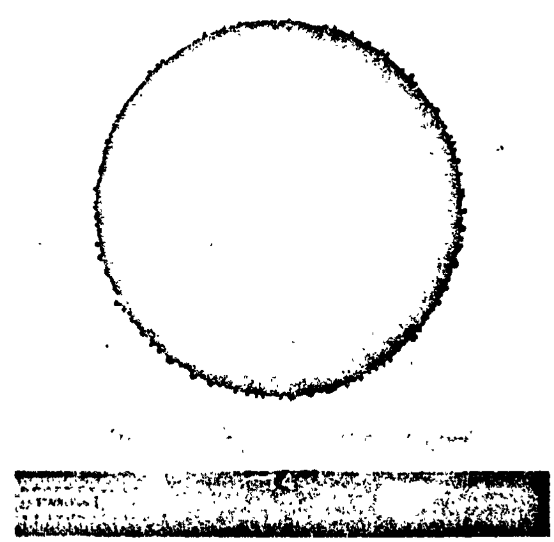

(b) After

Figure 18.- Photographs of Model 14 before and after arc jet test.

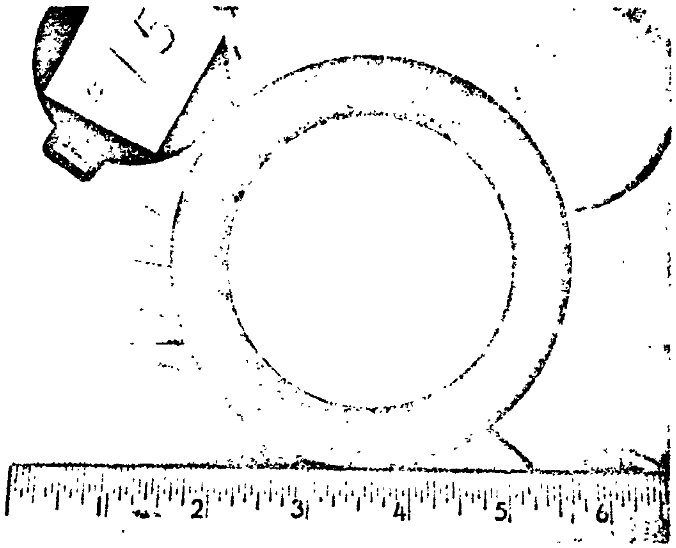

(a) Before

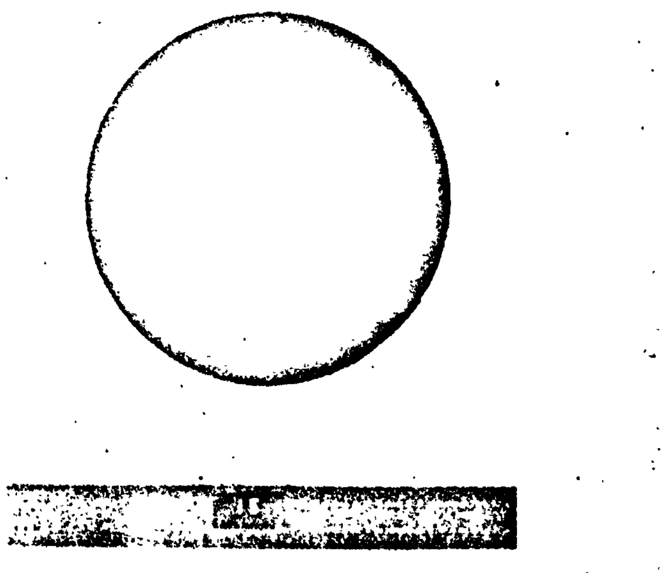

(b) After

Figure 19.- Photographs of Model 15 before and after arc jet test.

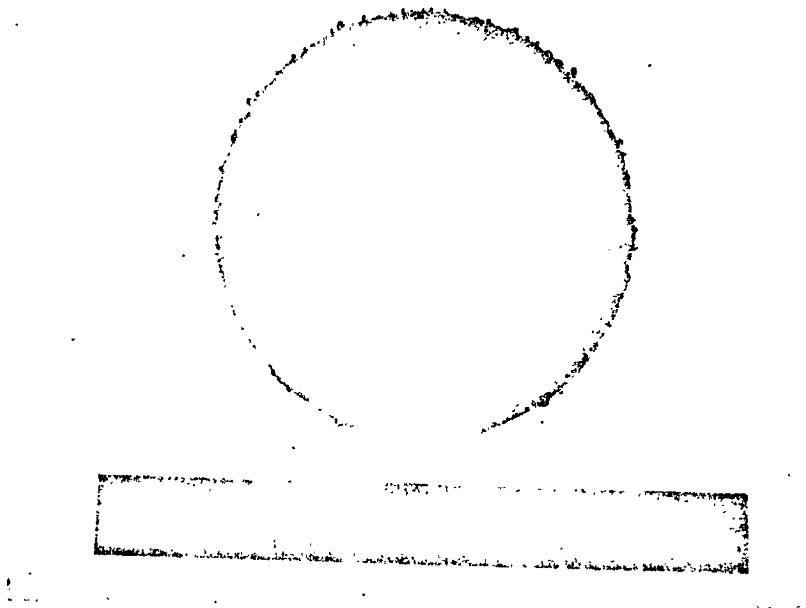

(a) Model 18

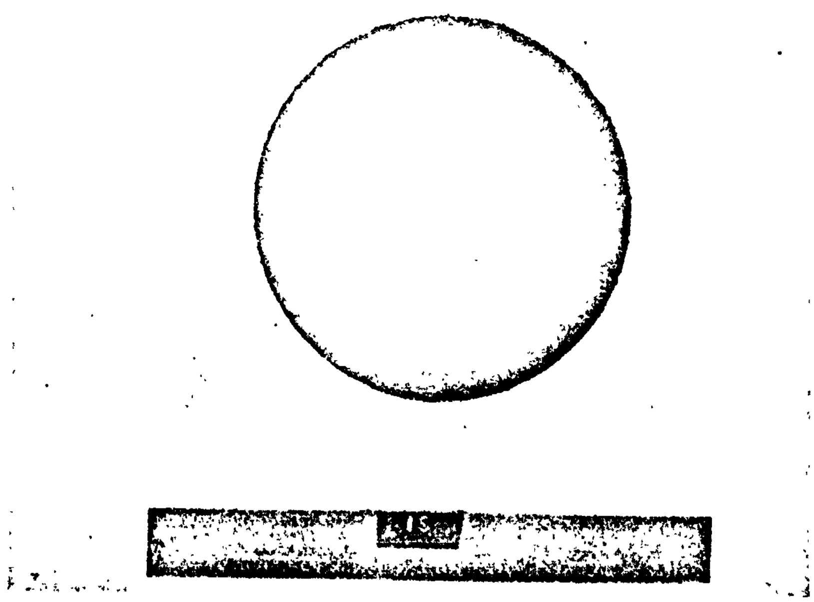

(b) Model 19

Figure 20.- Photographs of Models 18 and 19 after arc jet test.

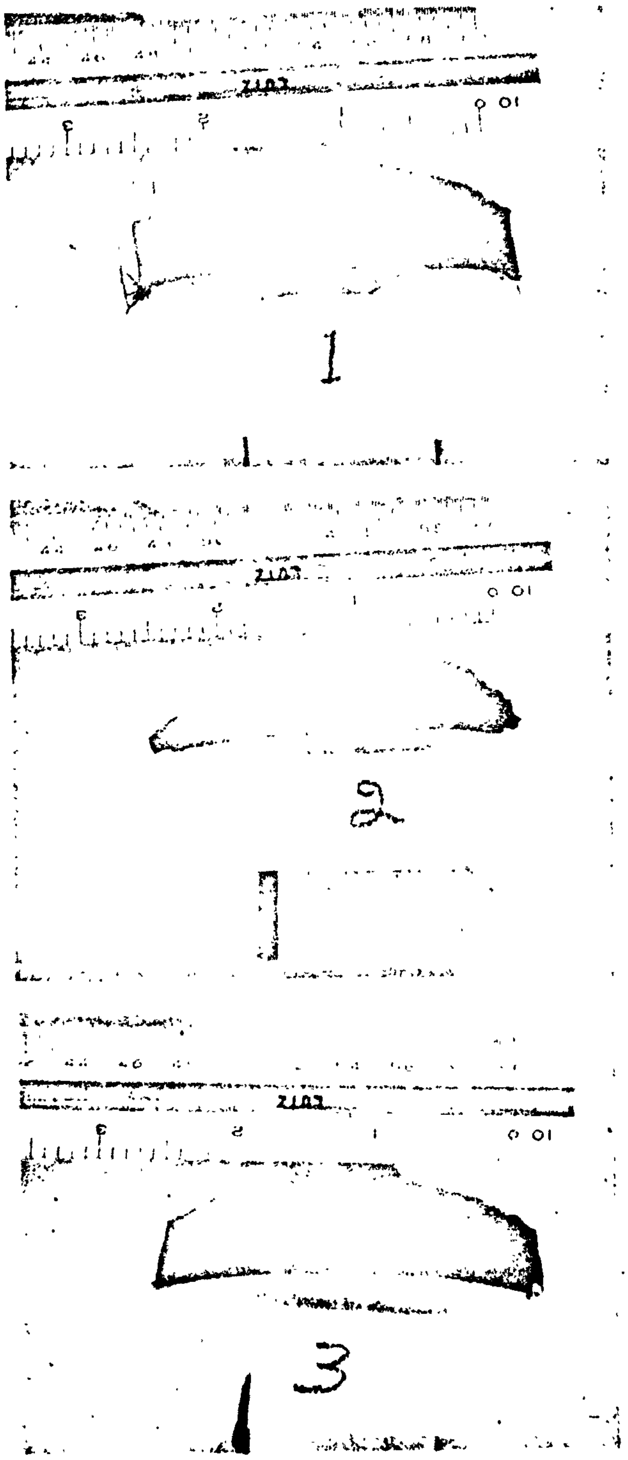

Figure 21.- Cross-sectioned views of models 1, 2, and 3 after arc jet tests.

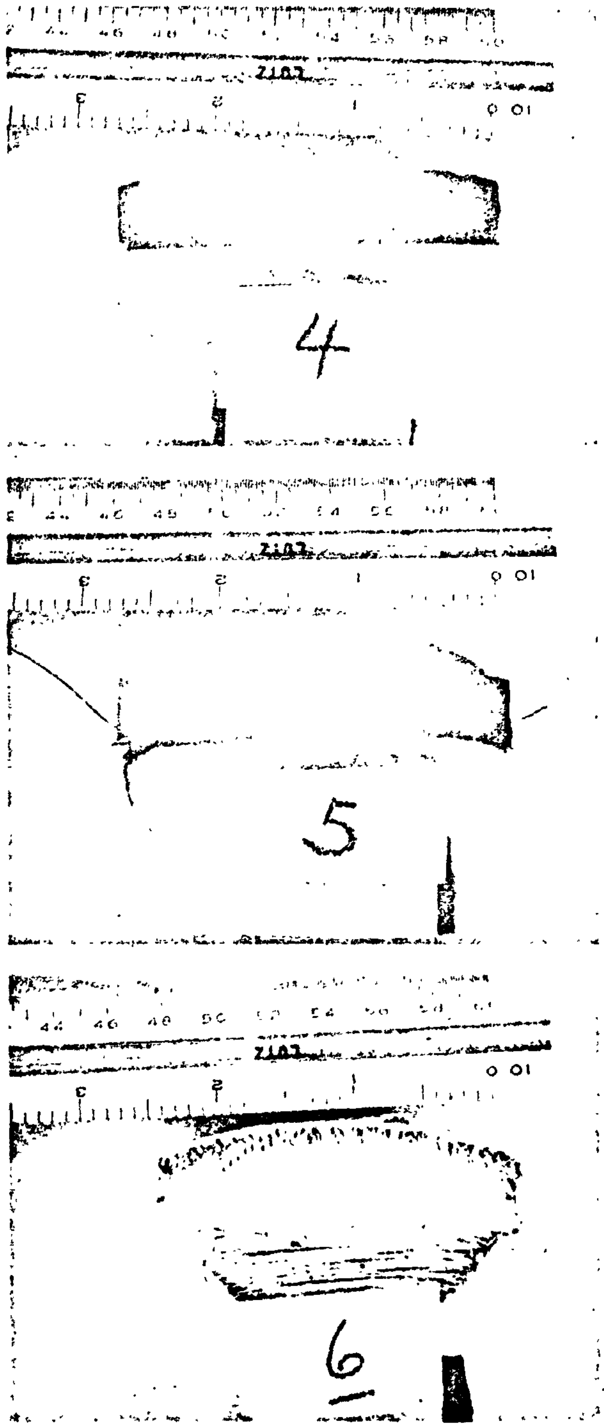

Figure 22.- Cross-sectioned views of models 4, 5, and 6 after arc jet tests.

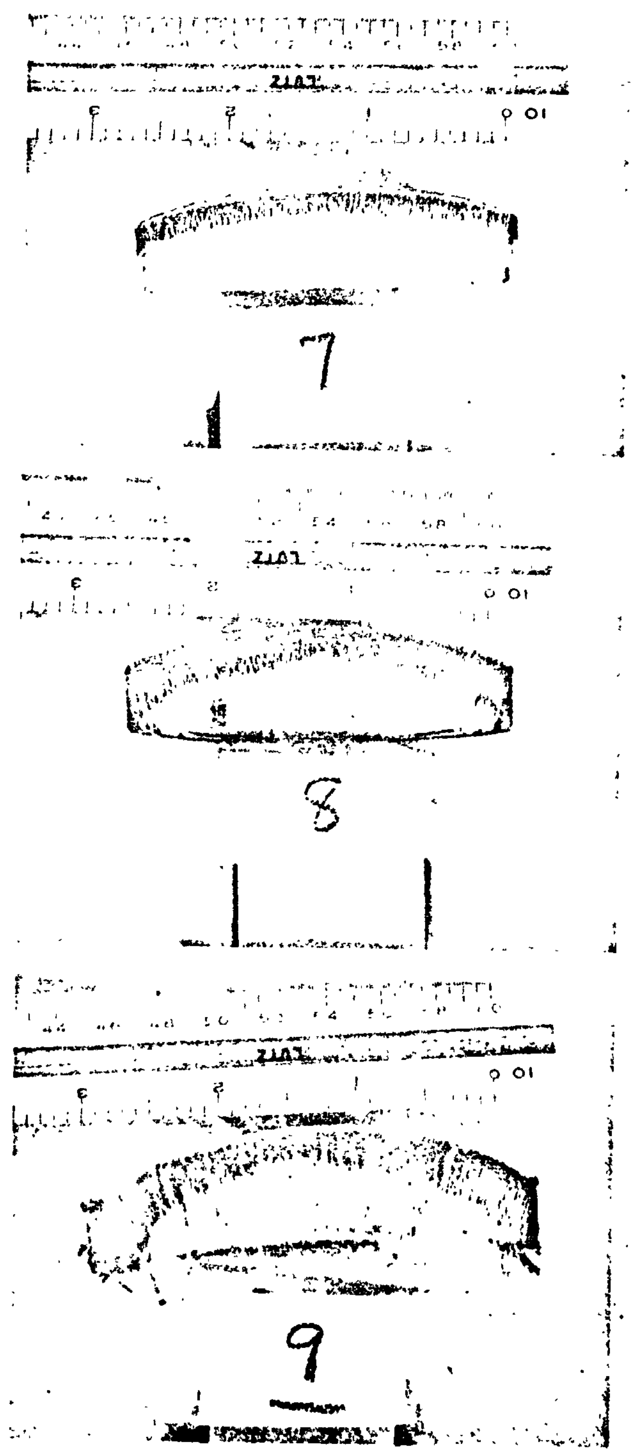

Figure 23.- Cross-sectioned views of models 7, 8, and 9 after arc jet tests.

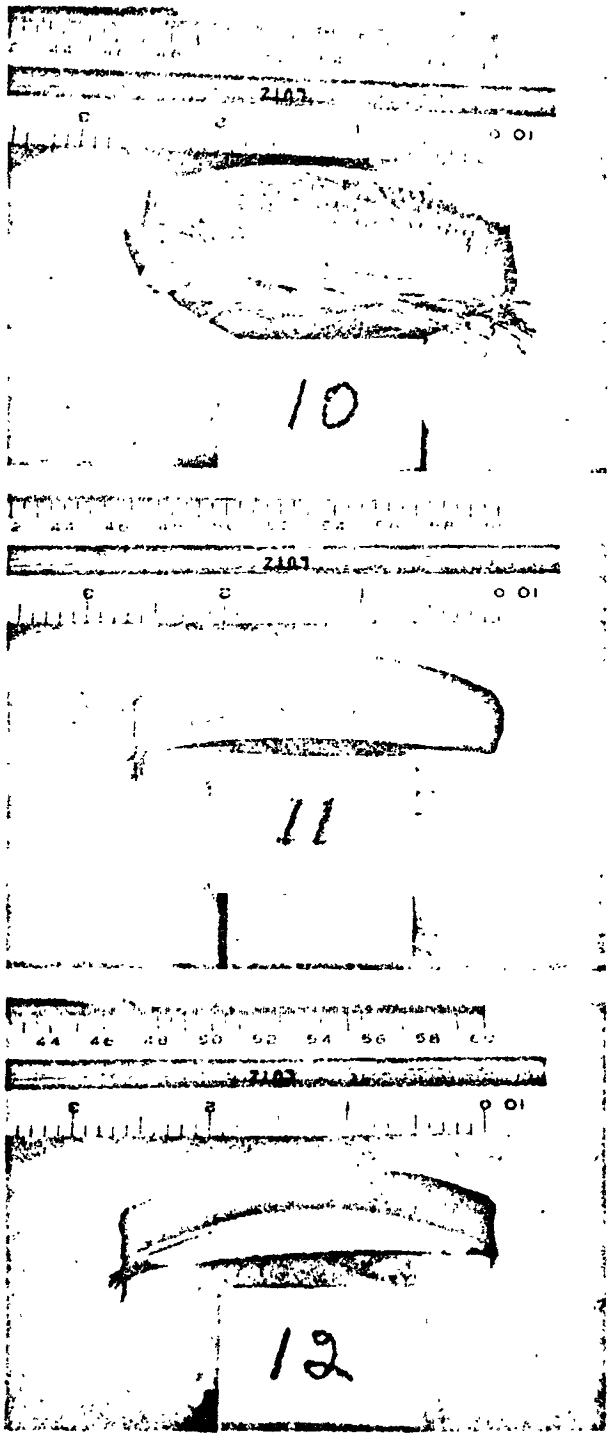

Figure 24.- Cross-sectioned views of models 10, 11, and 12 after arc jet tests.

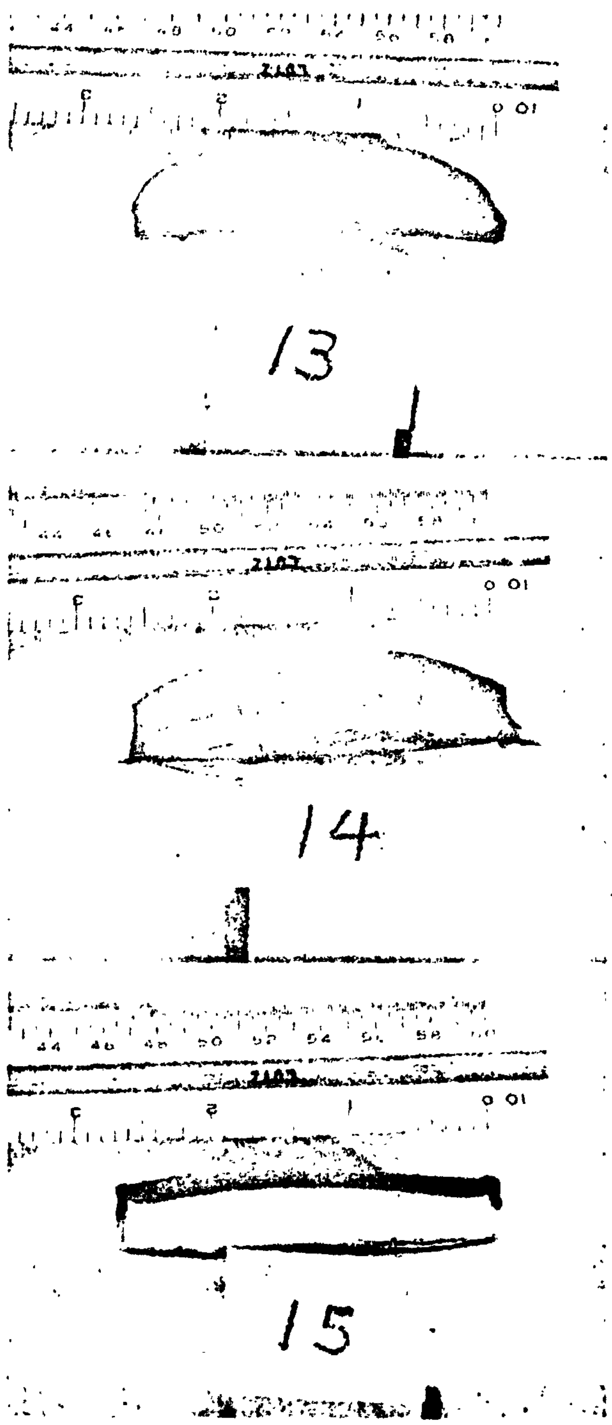

Figure 25.- Cross-sectioned views of models 13, 14, and 15 after arc jet tests.

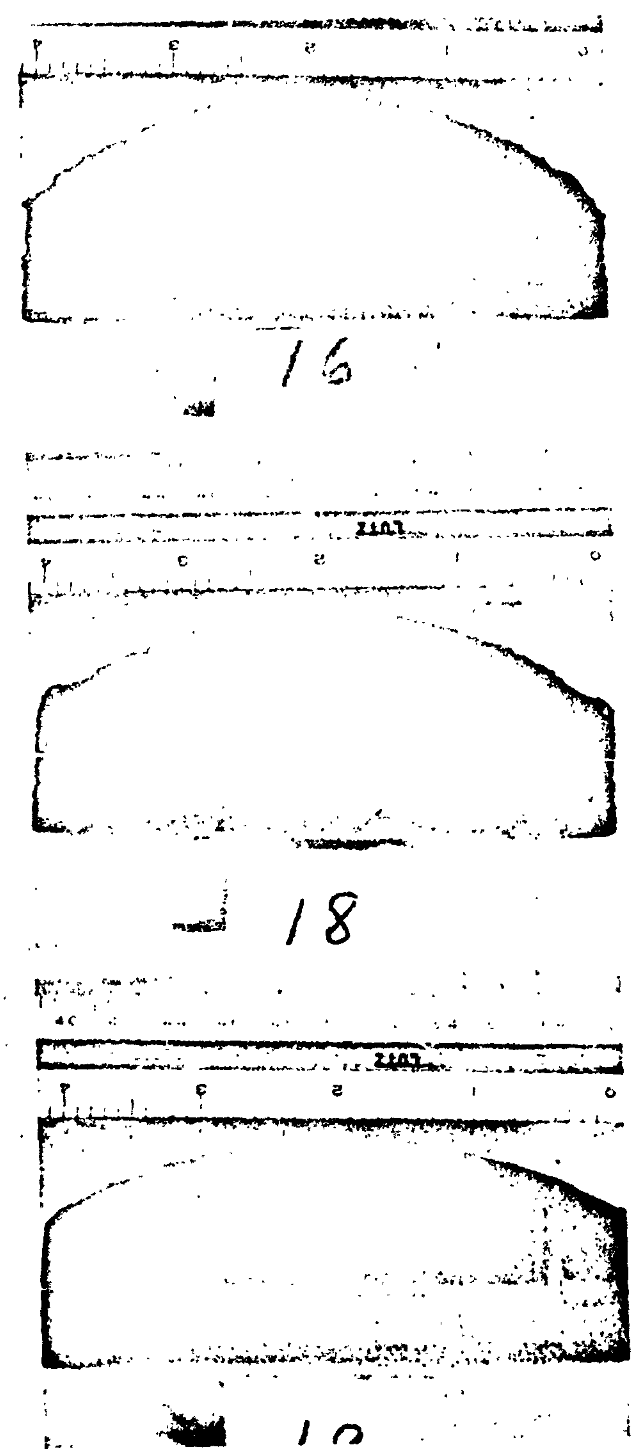

Figure 26.- Cross-sectioned views of models 16, 18, and 19 after arc jet tests.

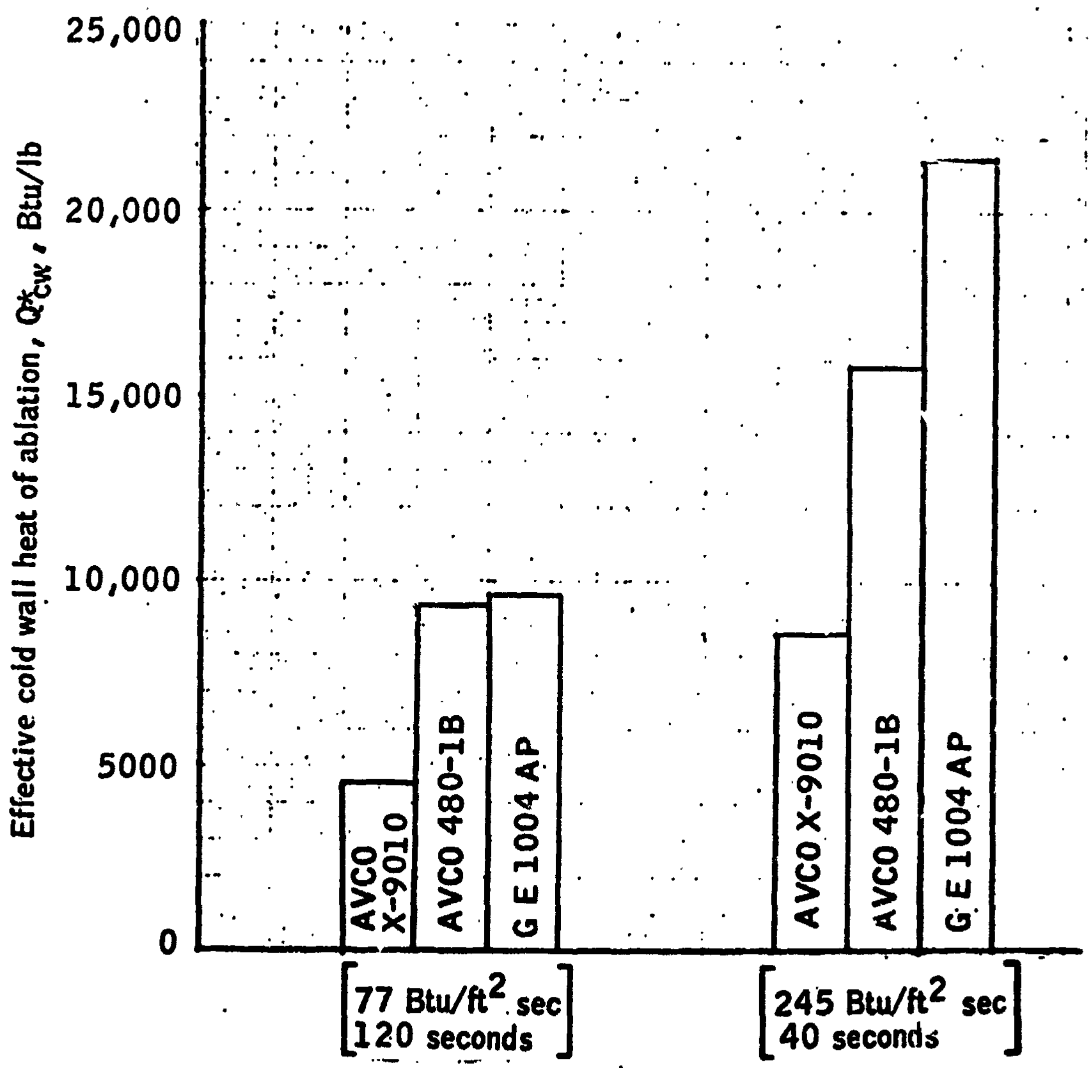

Figure 27.- Relative thermal efficiency of three ablators at two steady state heating conditions.

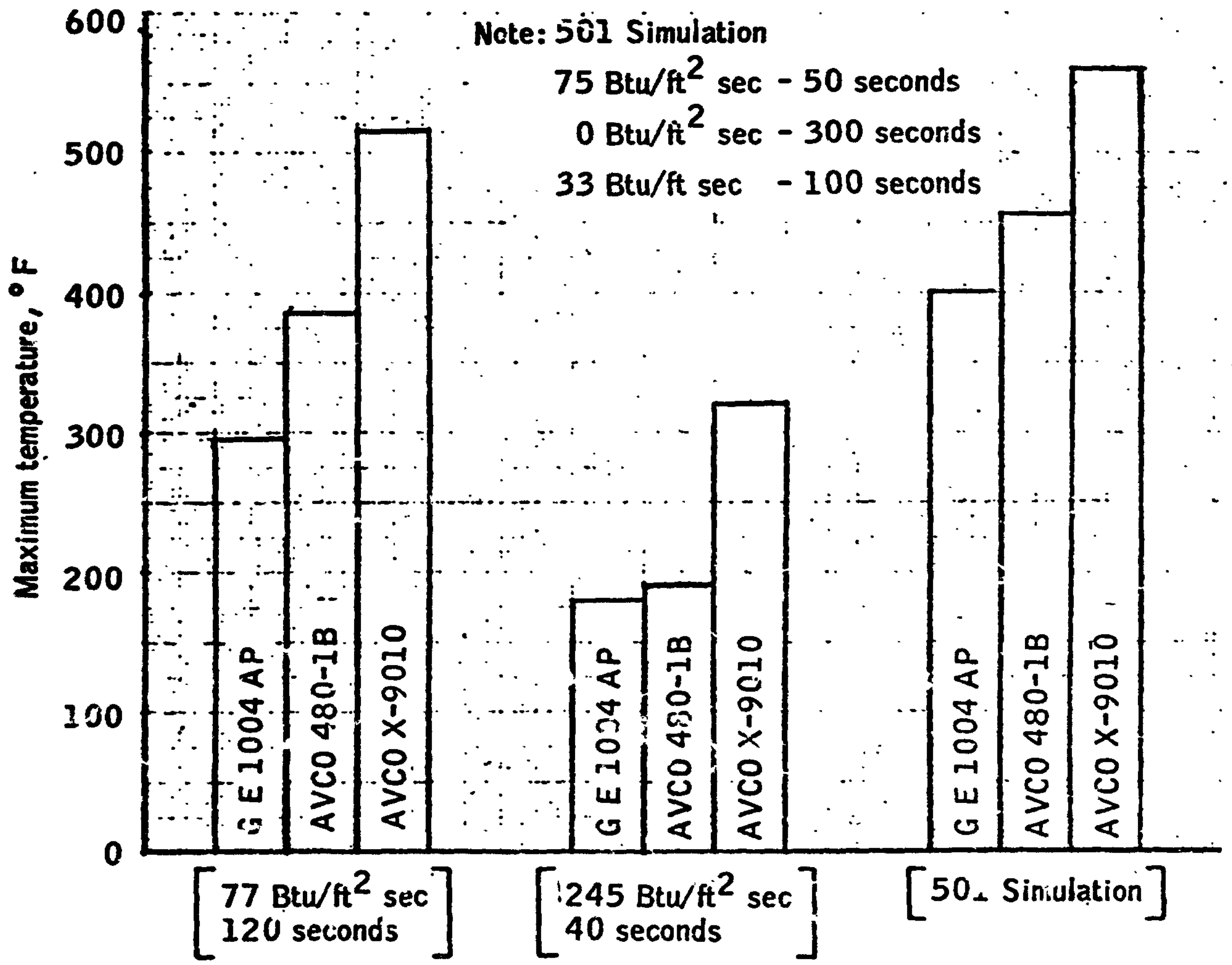

Figure 28.- Maximum backface temperatures of three ablators for three test environments.

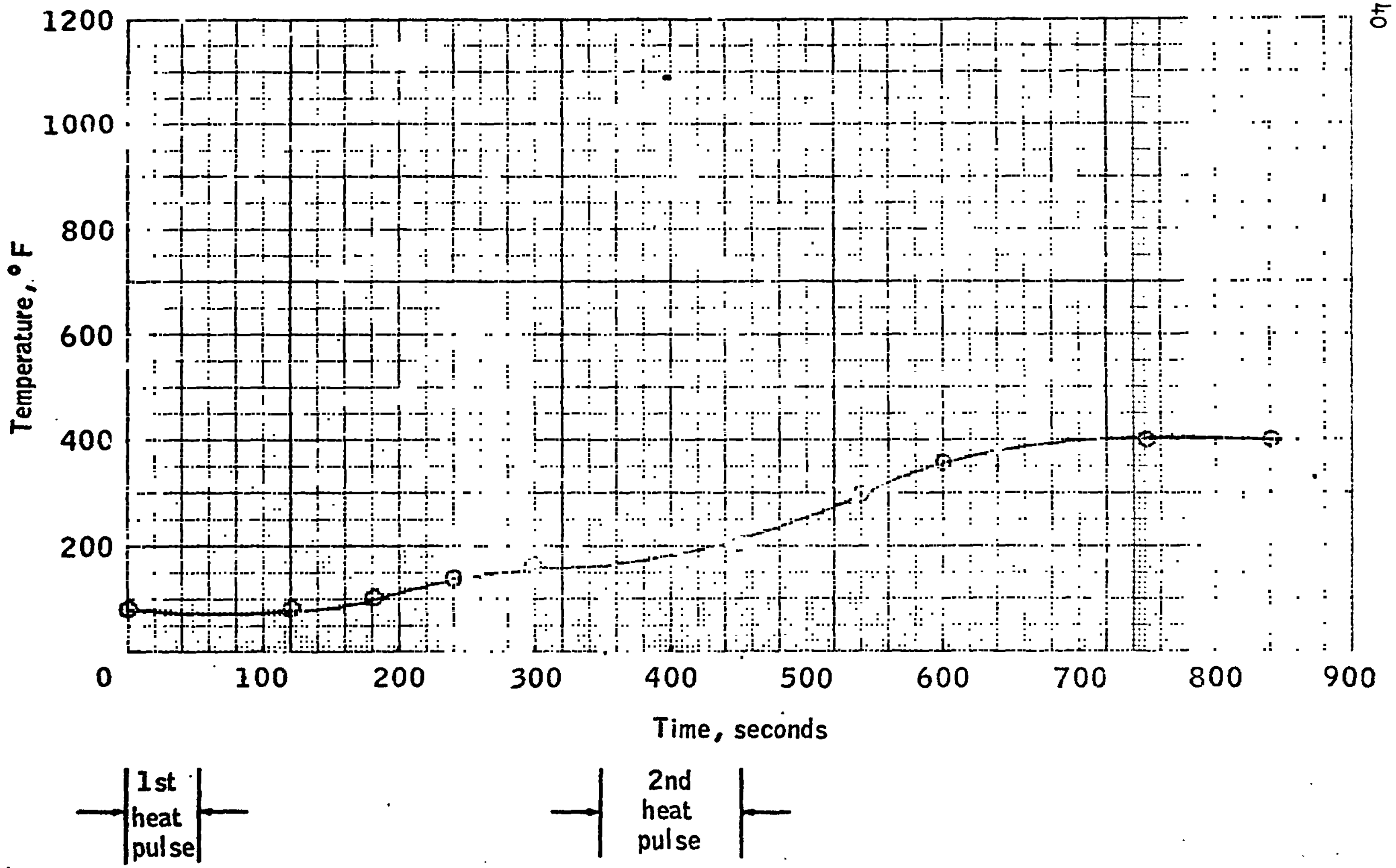

Figure 29.- Backface temperature-time history of model 1.

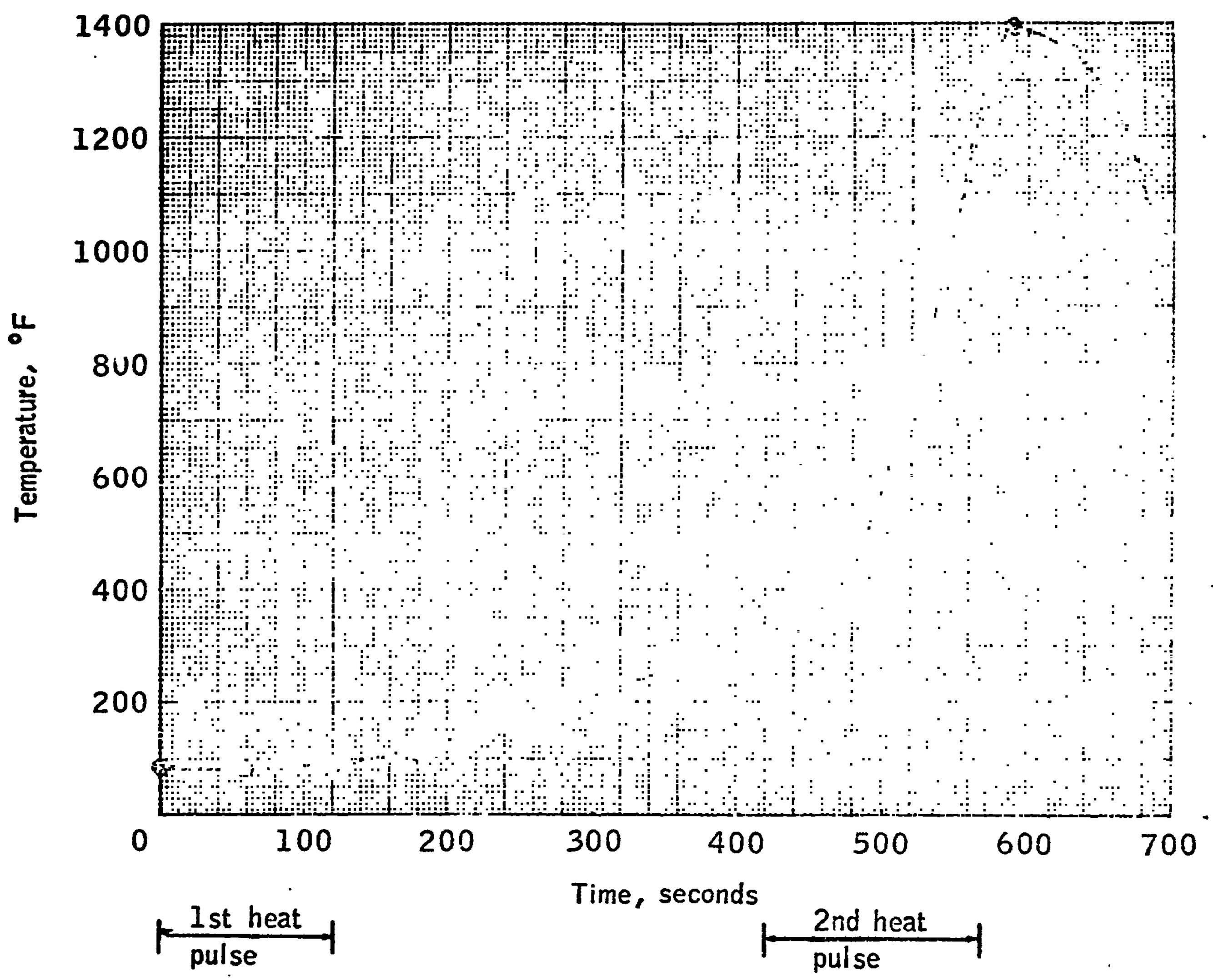

Figure 30.- Backface temperature-time history of model 2.

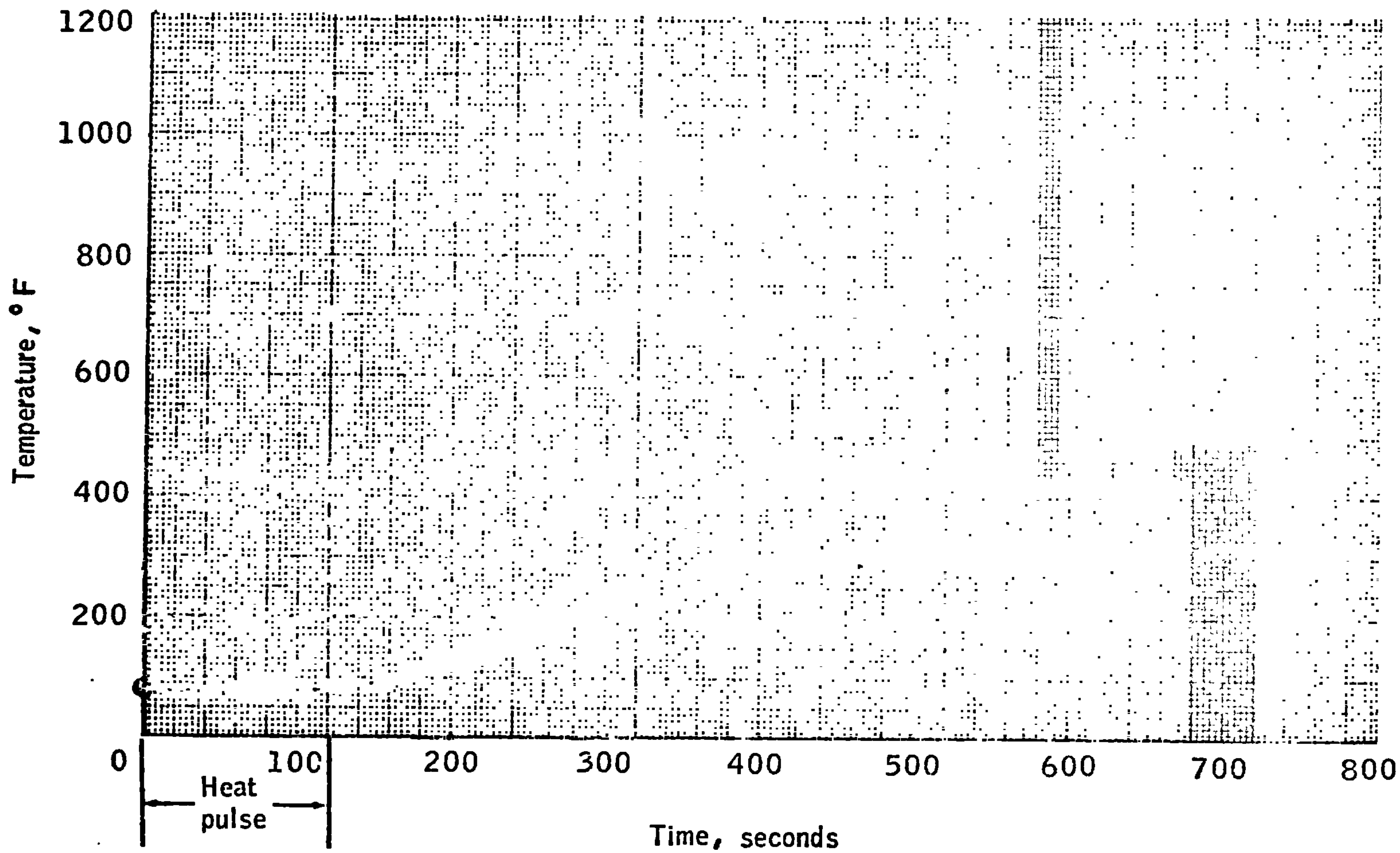

Figure 31.- Backface temperature-time history of model 3.

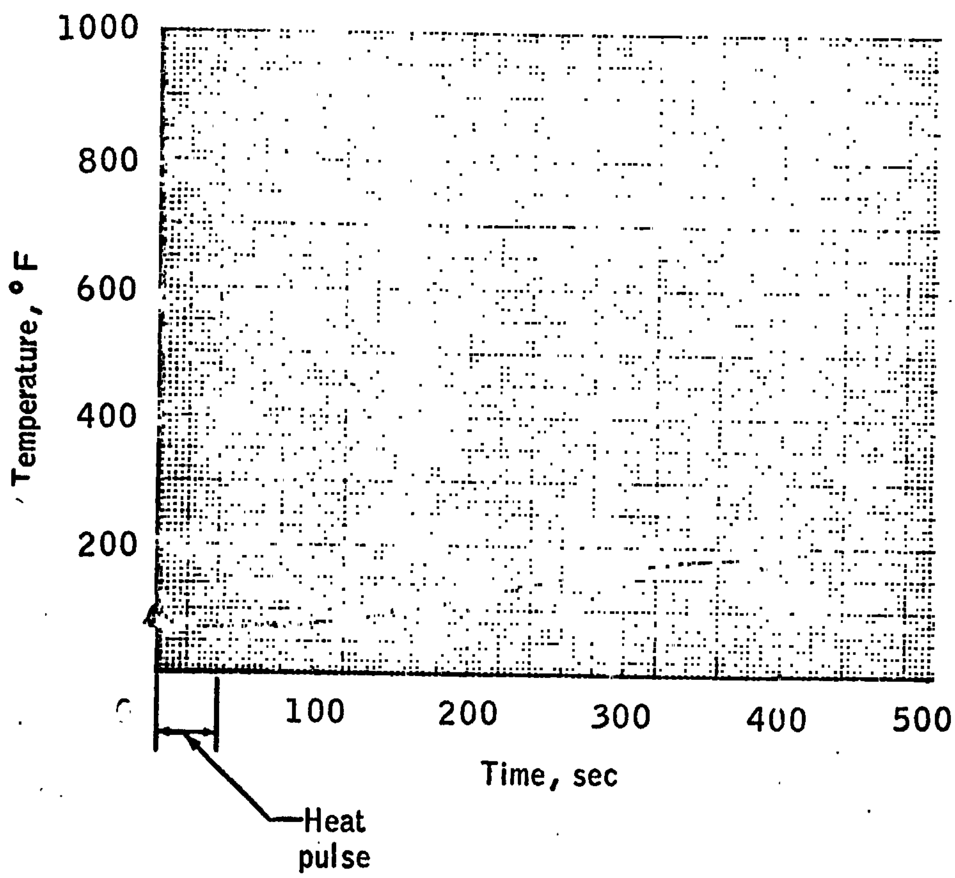

Figure 32.- Backface temperature-time history of model 4.

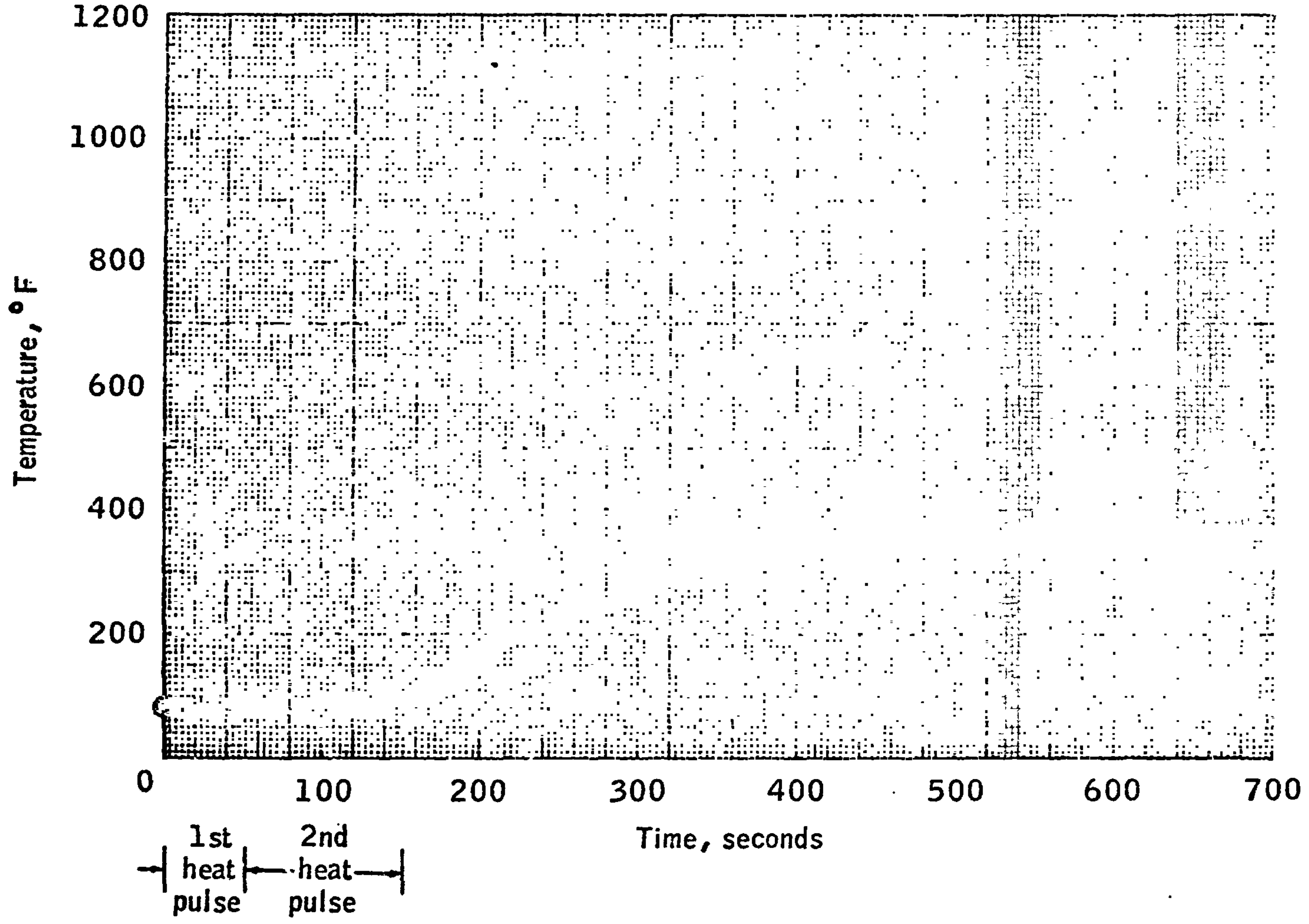

Figure 33.- Backface temperature-time history of model 5.

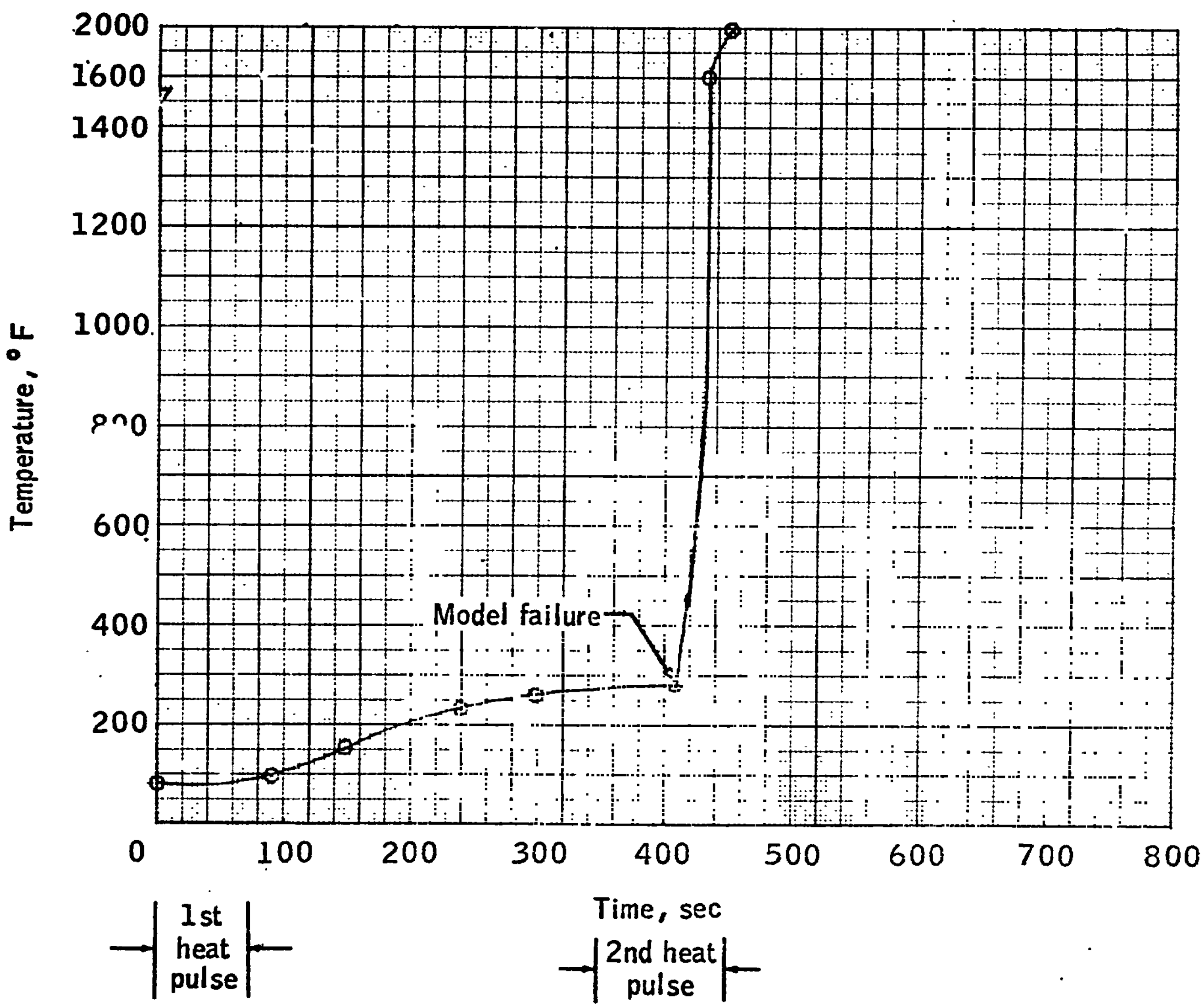

Figure 34.- Backface temperature-time history of model 6.

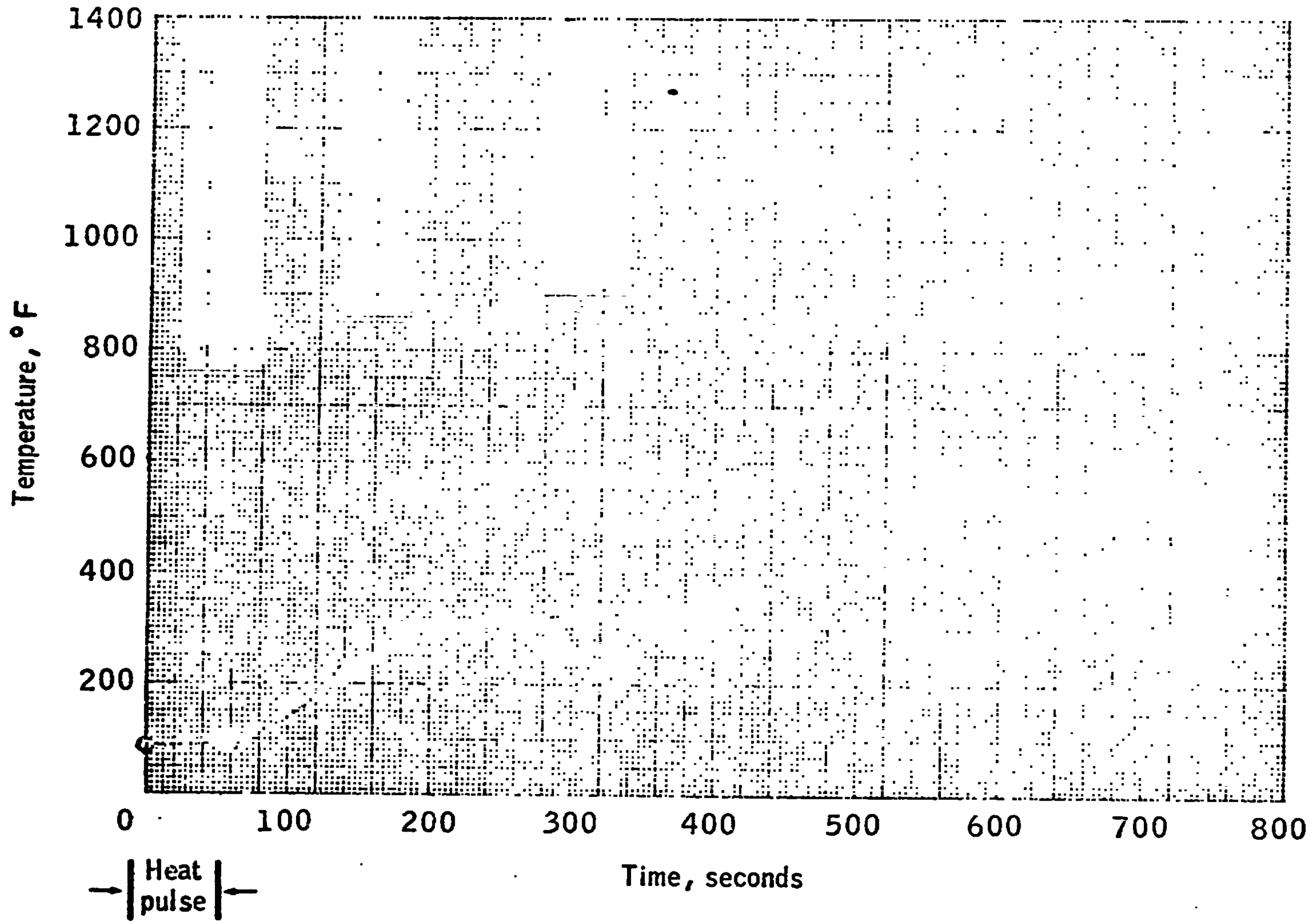

Figure 35.- Backface temperature-time history of model 7.

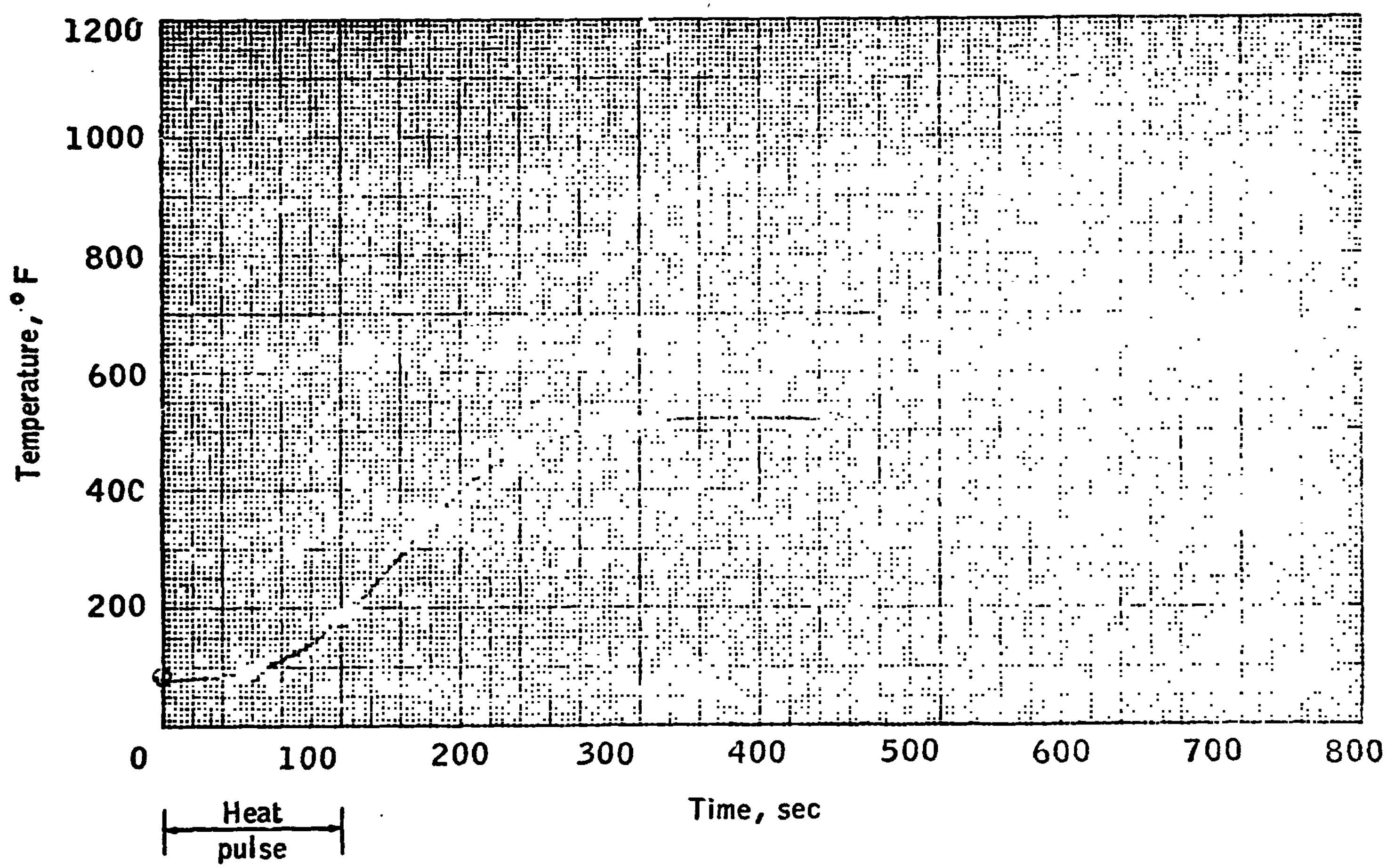

Figure 36.- Backface temperature-time history of model 8.

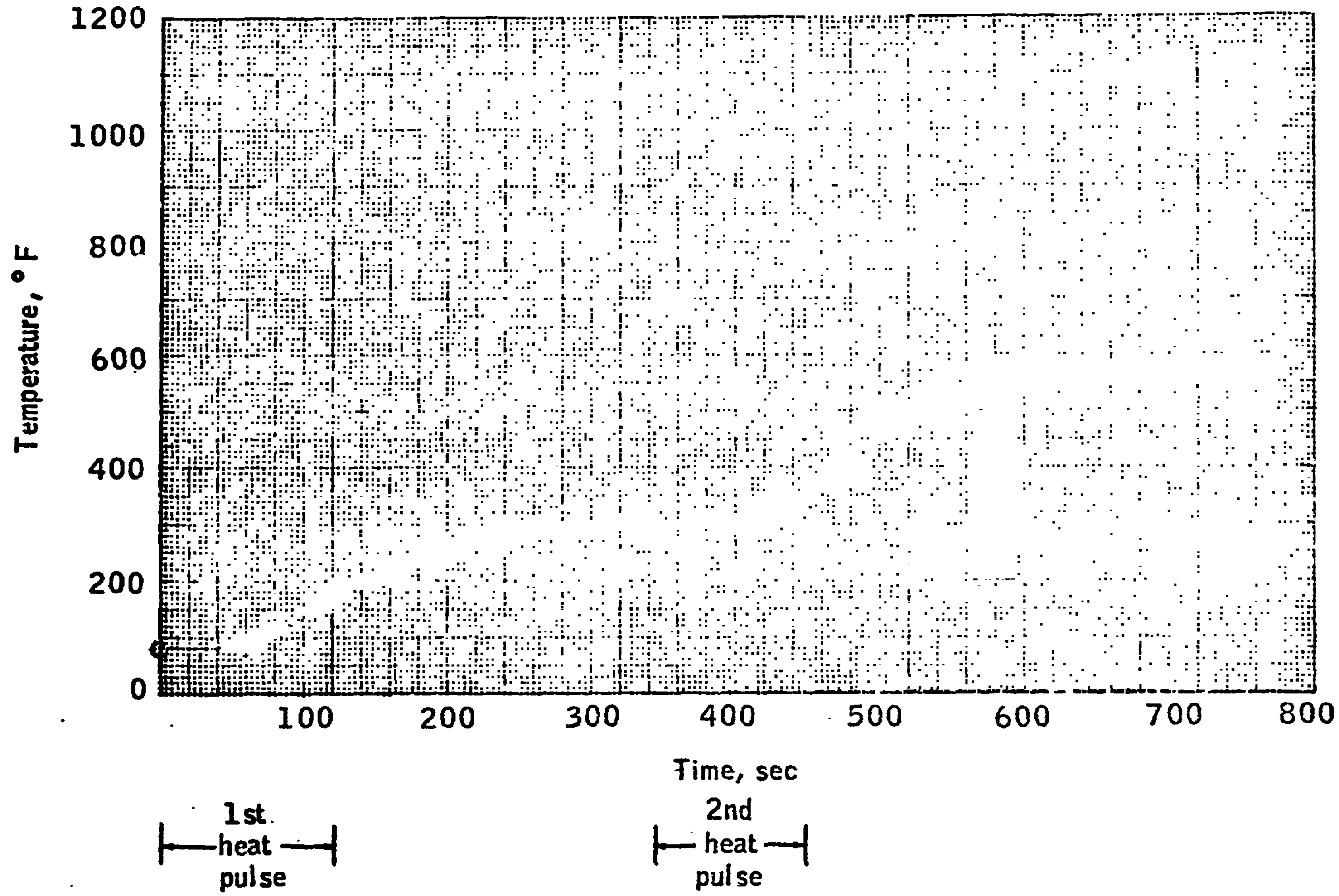

Figure 37.- Backface temperature-time history of model 9.

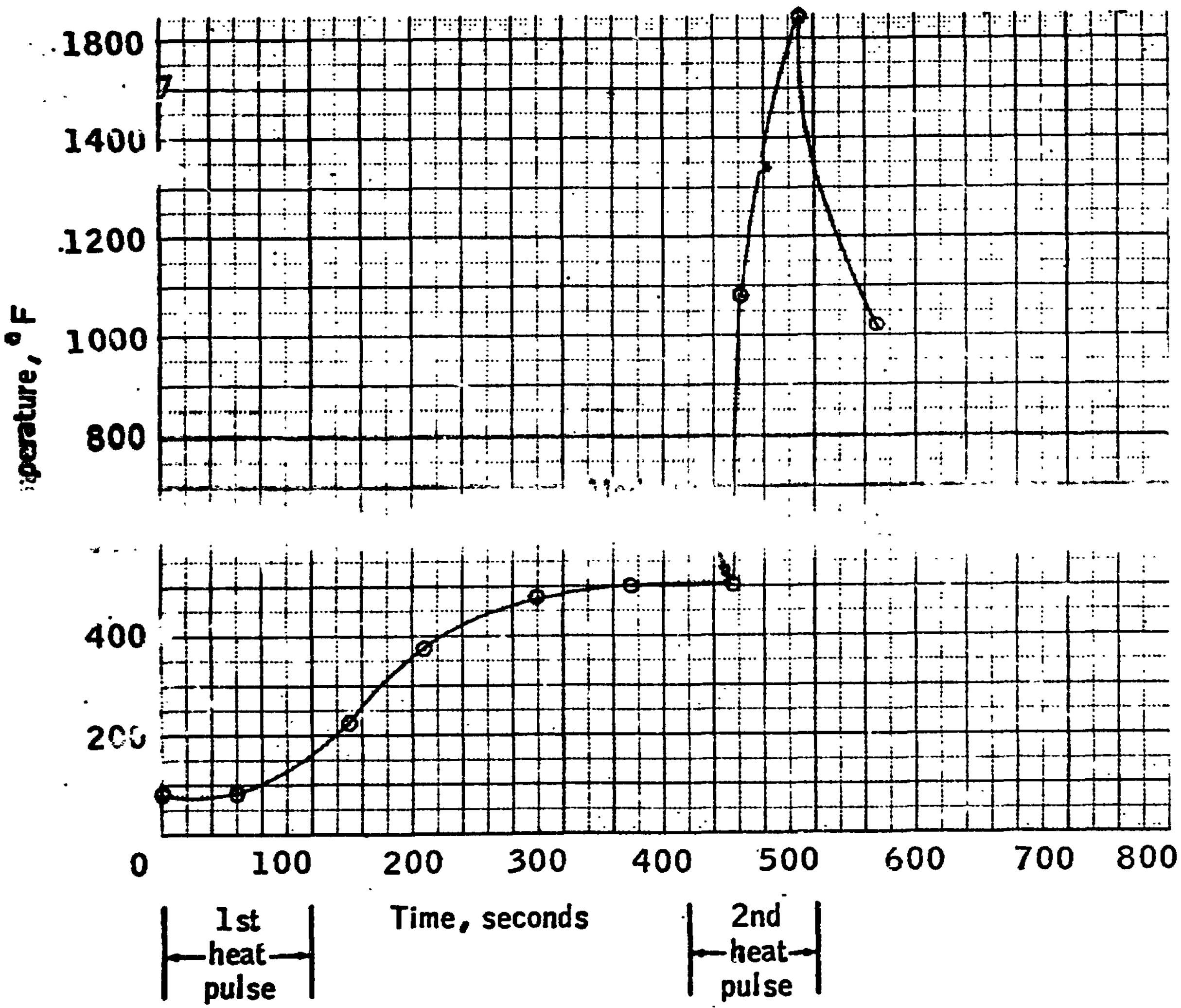

Figure 38.- Backface temperature-time history of model 10.

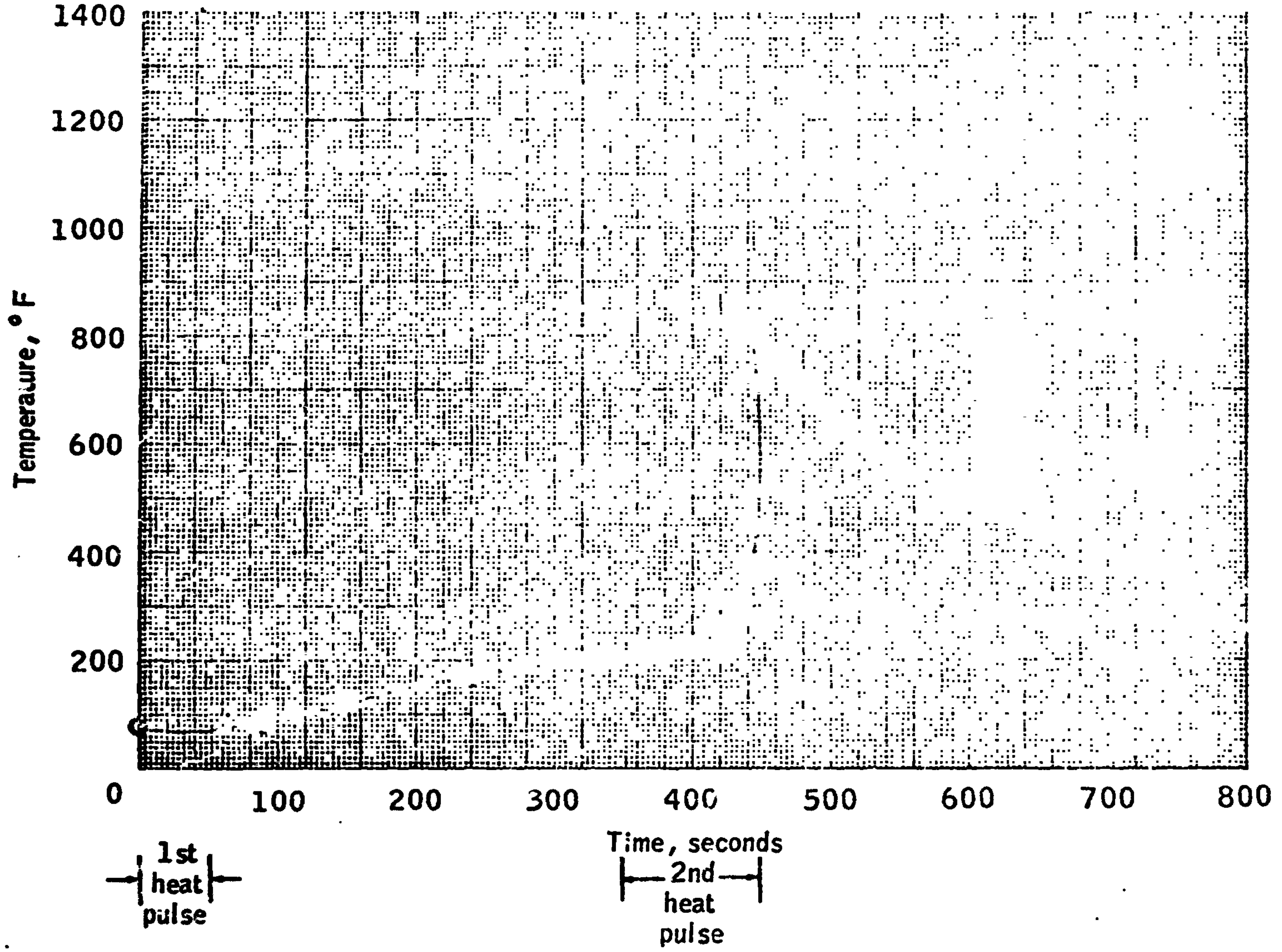

Figure 39.- Backface temperature-time history of model 11.

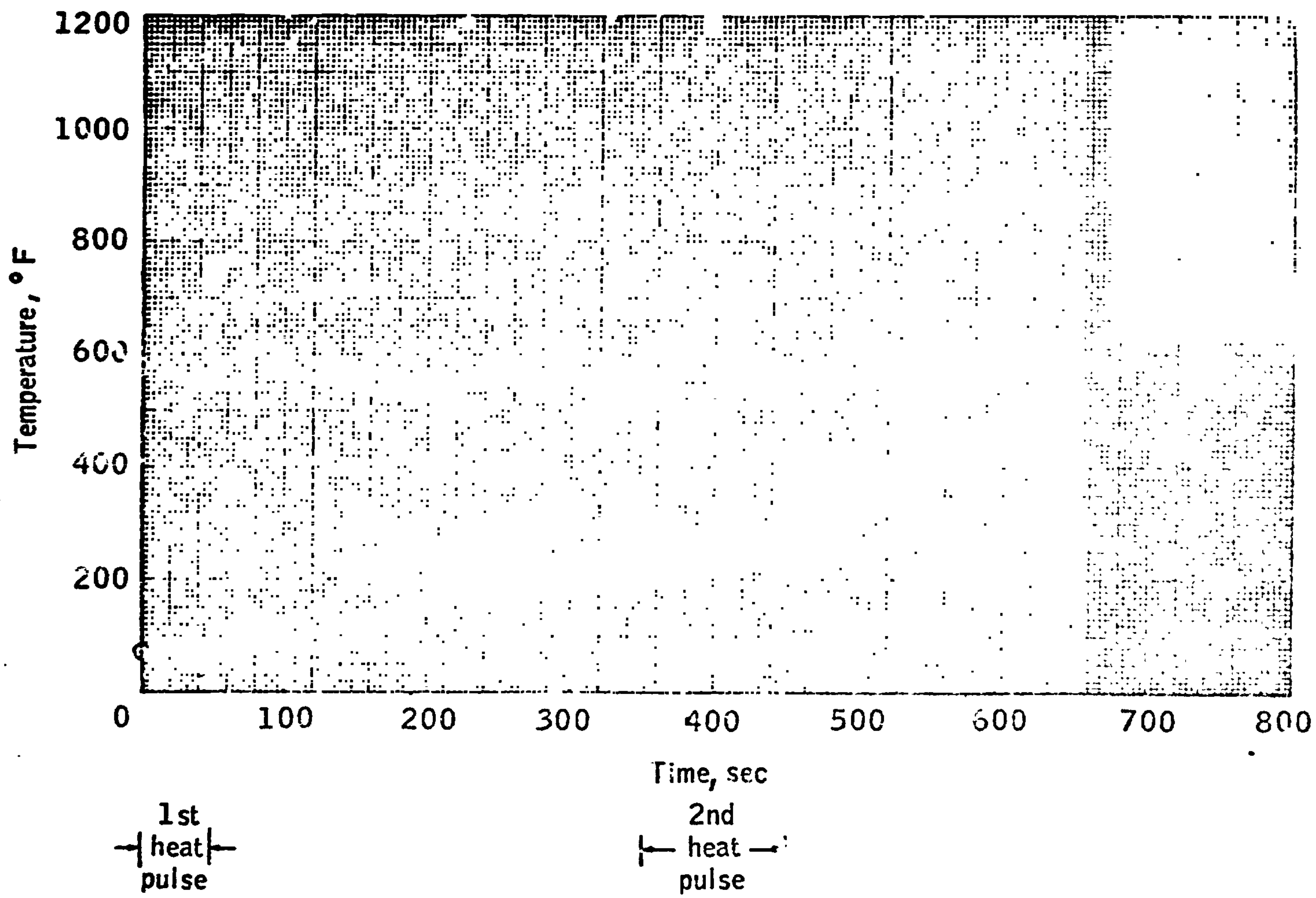

Figure 40 Backface temperature-time history of model 12.

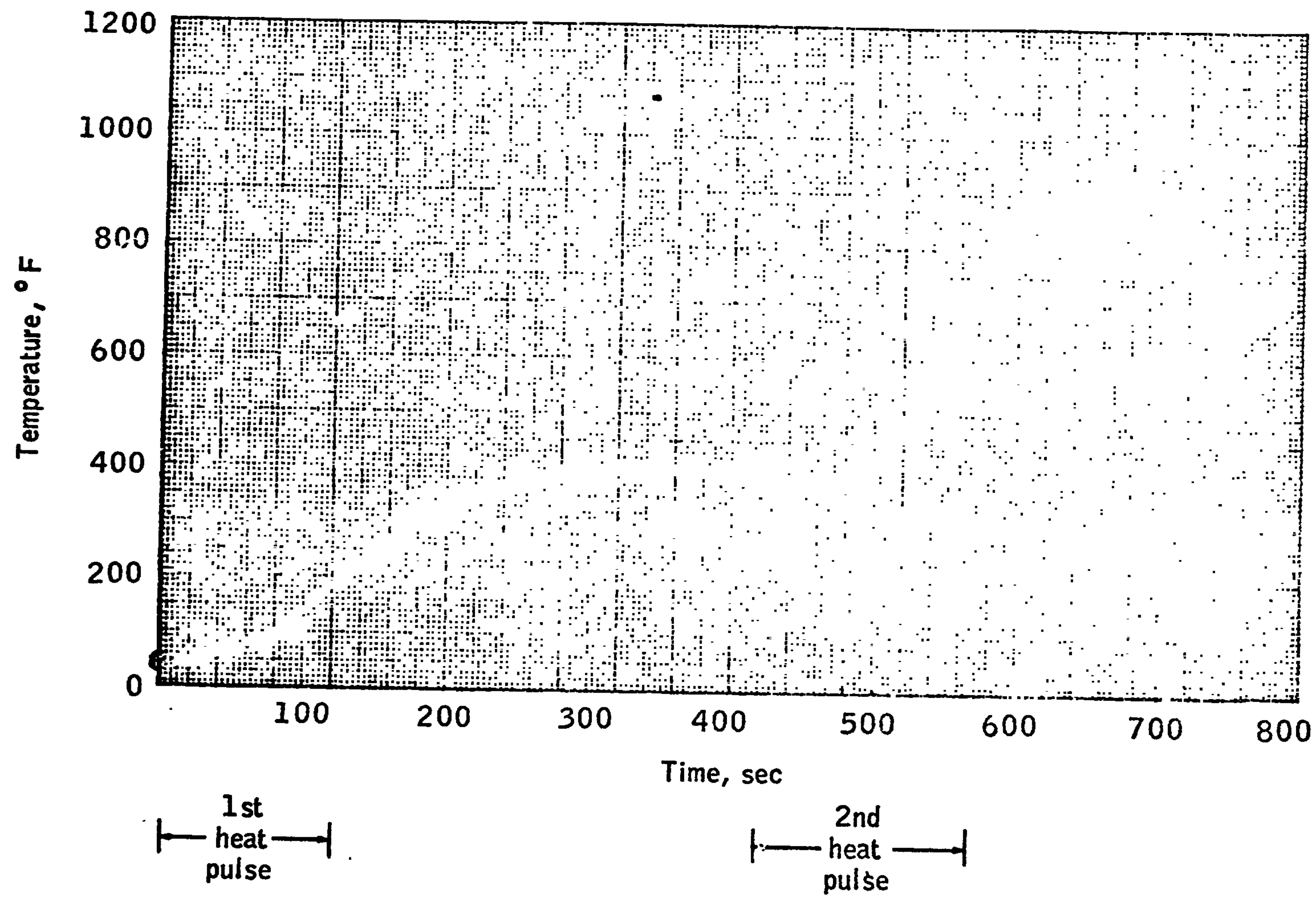

Figure 41.- Backface temperature-time history of model 13.

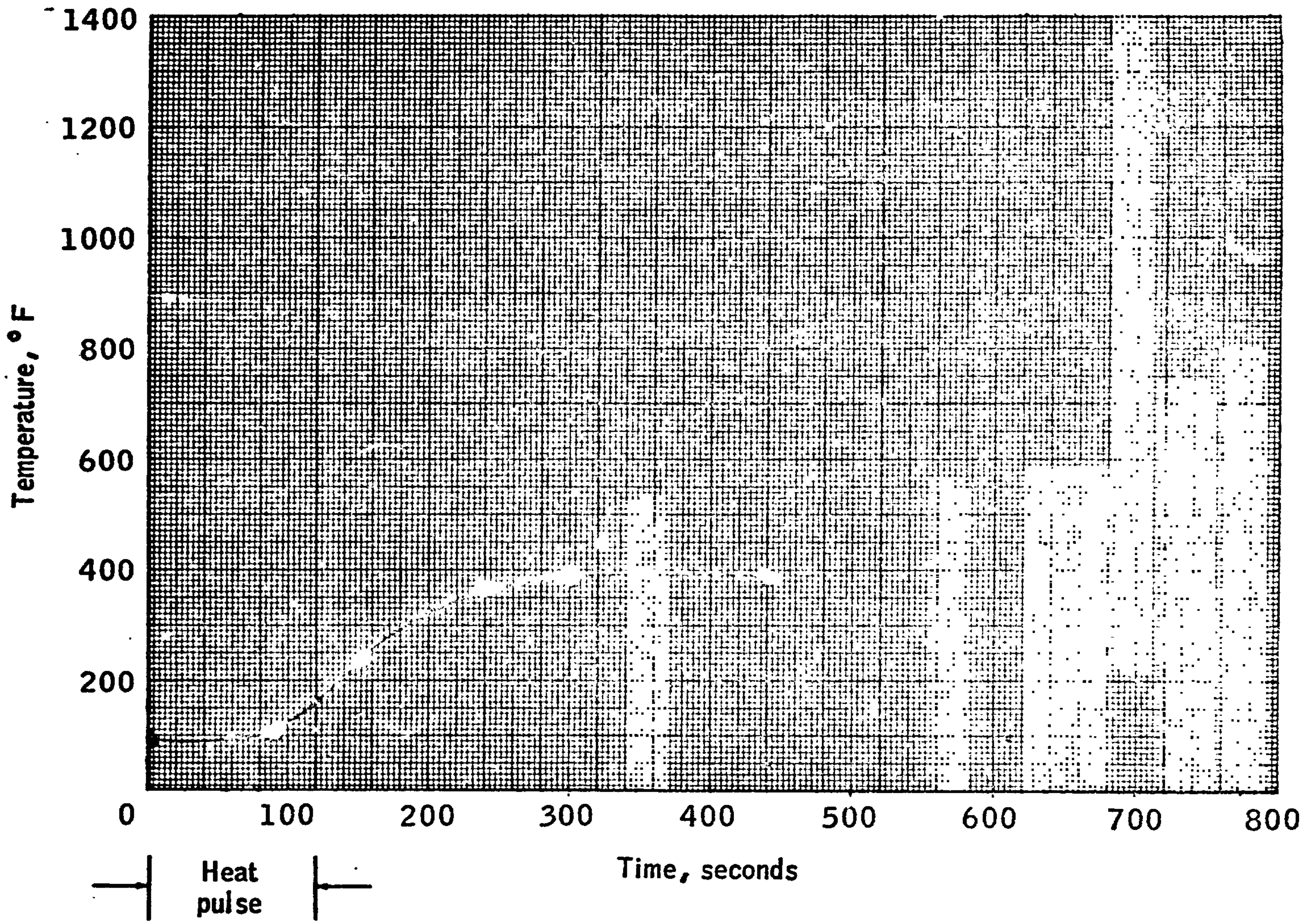

Figure 42.- Backface temperature-time history of model 14.

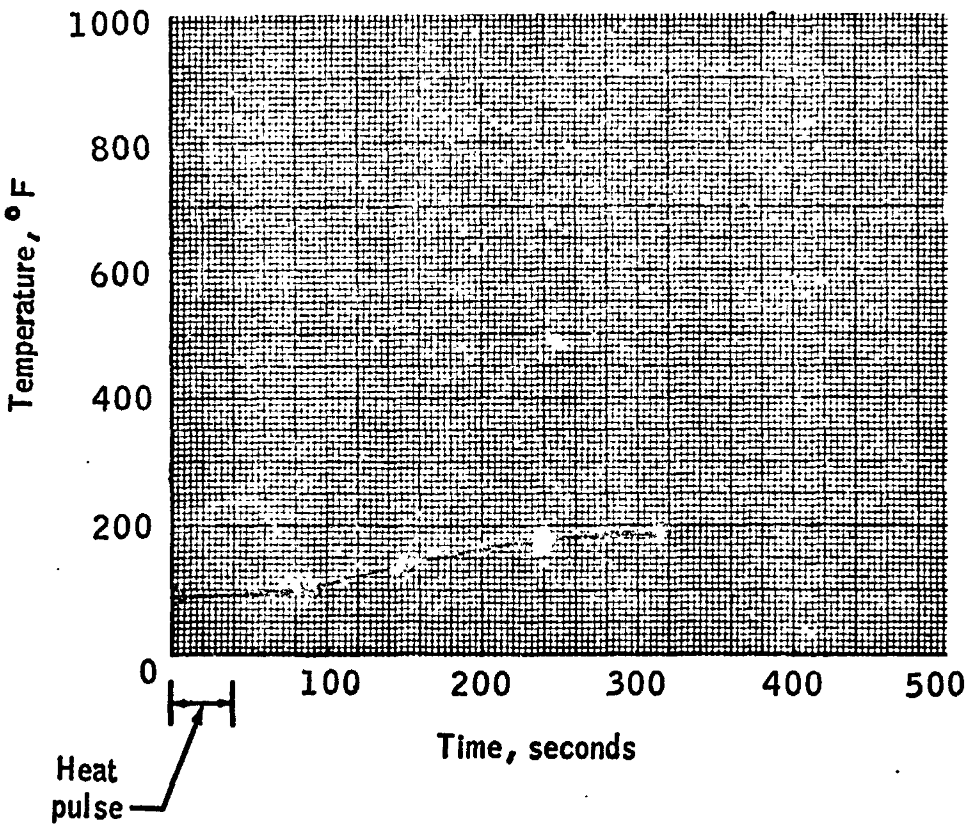

Figure 43.- Backface temperature-time history of model 15.

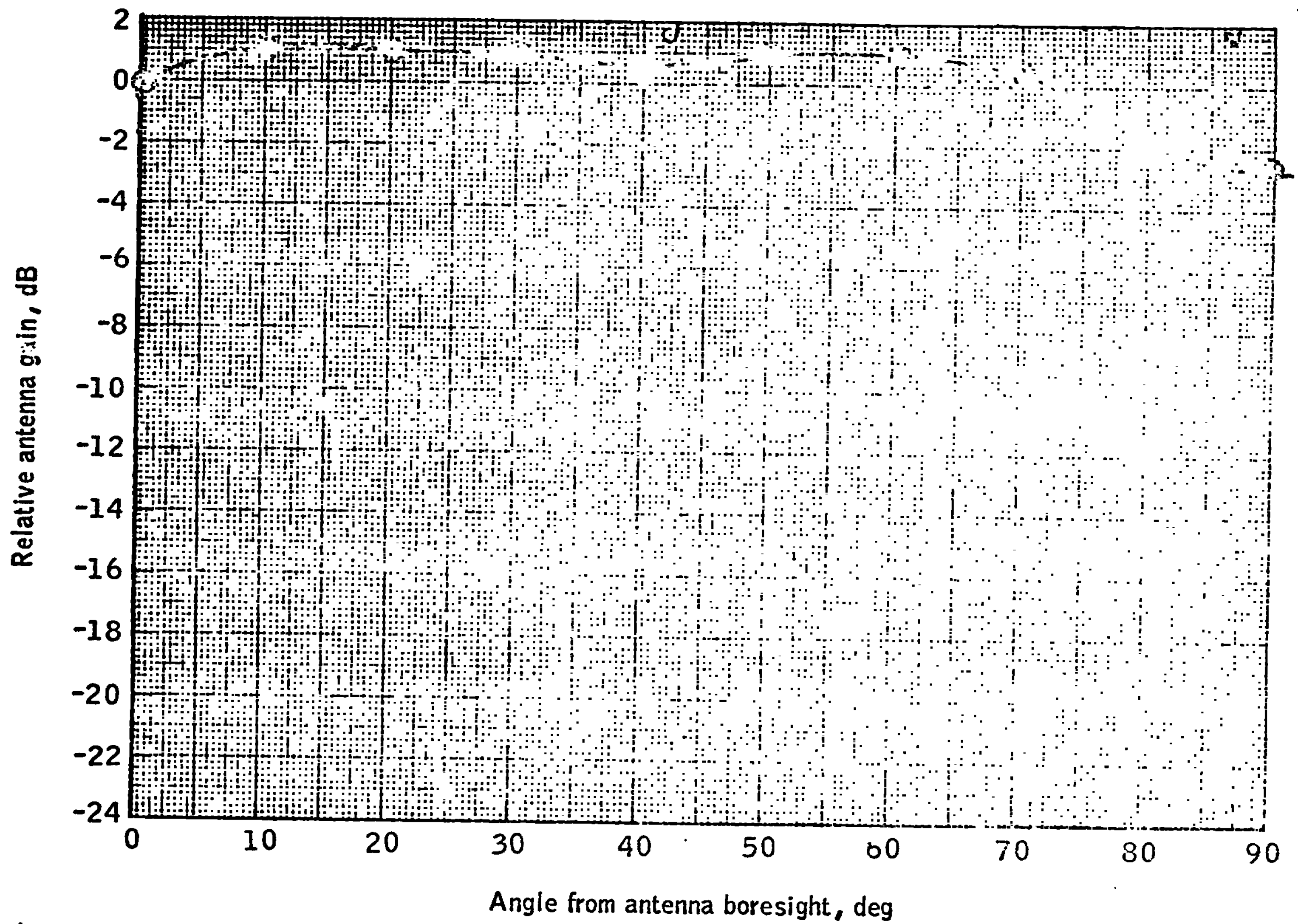

Figure 44.- Gain of CSM antenna covered by Model 1 before arc jet test with reference to uncovered CSM antenna versus the angle from the antenna boresight.

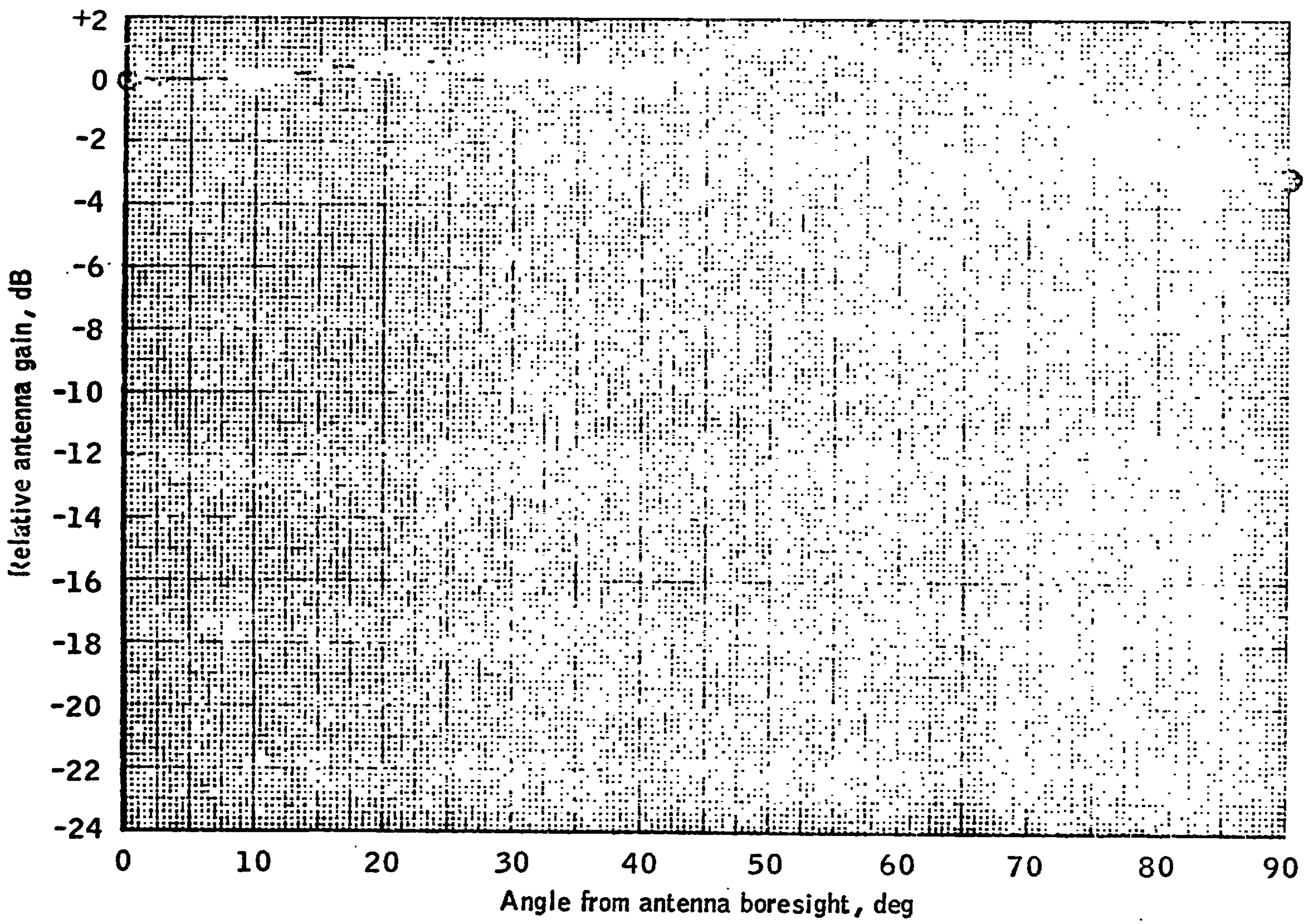

Figure 45.- Gain of CSM antenna covered by Model 7 before arc jet test with reference to uncovered CSM antenna versus the angle from the antenna boresight.

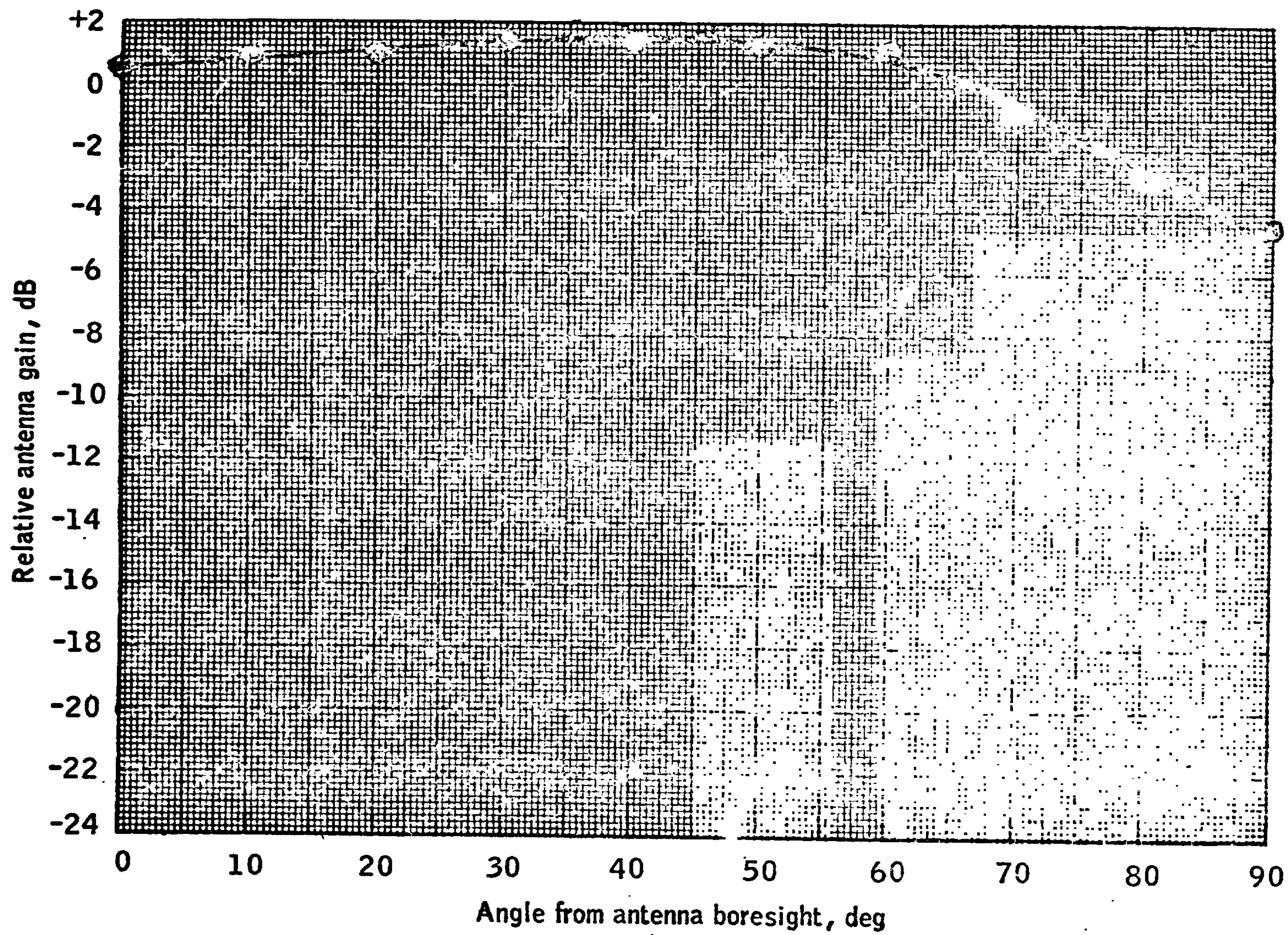

Figure 46.- Gain of CSM antenna covered by Model 11 before arc jet test with reference to uncovered CSM antenna versus the angle from the antenna boresight.

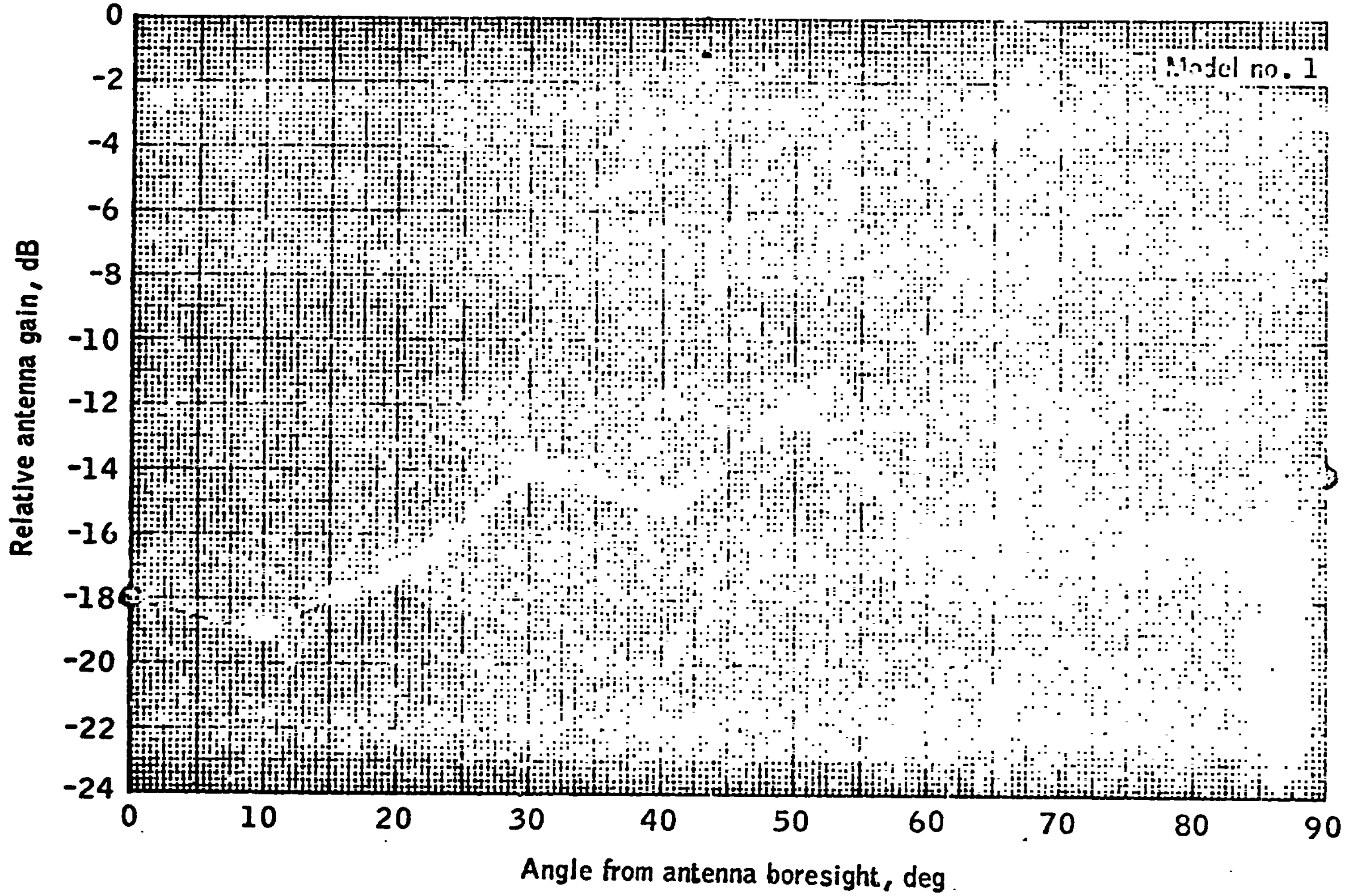

Figure 47.- Gain of CSM antenna covered by Model 1 after arc jet test with reference to uncovered CSM antenna versus the angle from the antenna boresight.

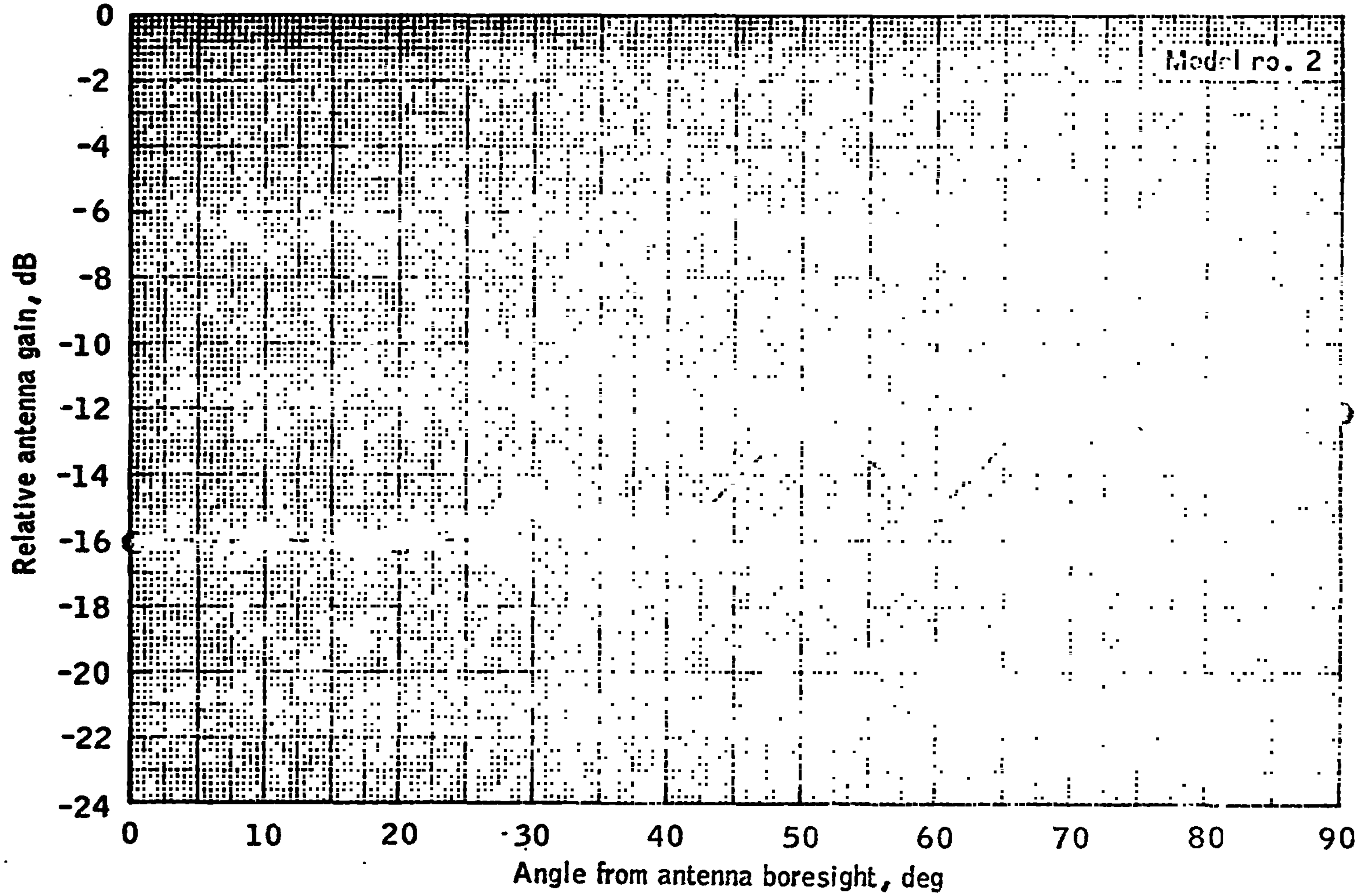

Figure 48.- Gain of CSM antenna covered by Model 2 after arc jet test with reference to uncovered CSM antenna versus the angle from the antenna boresight.

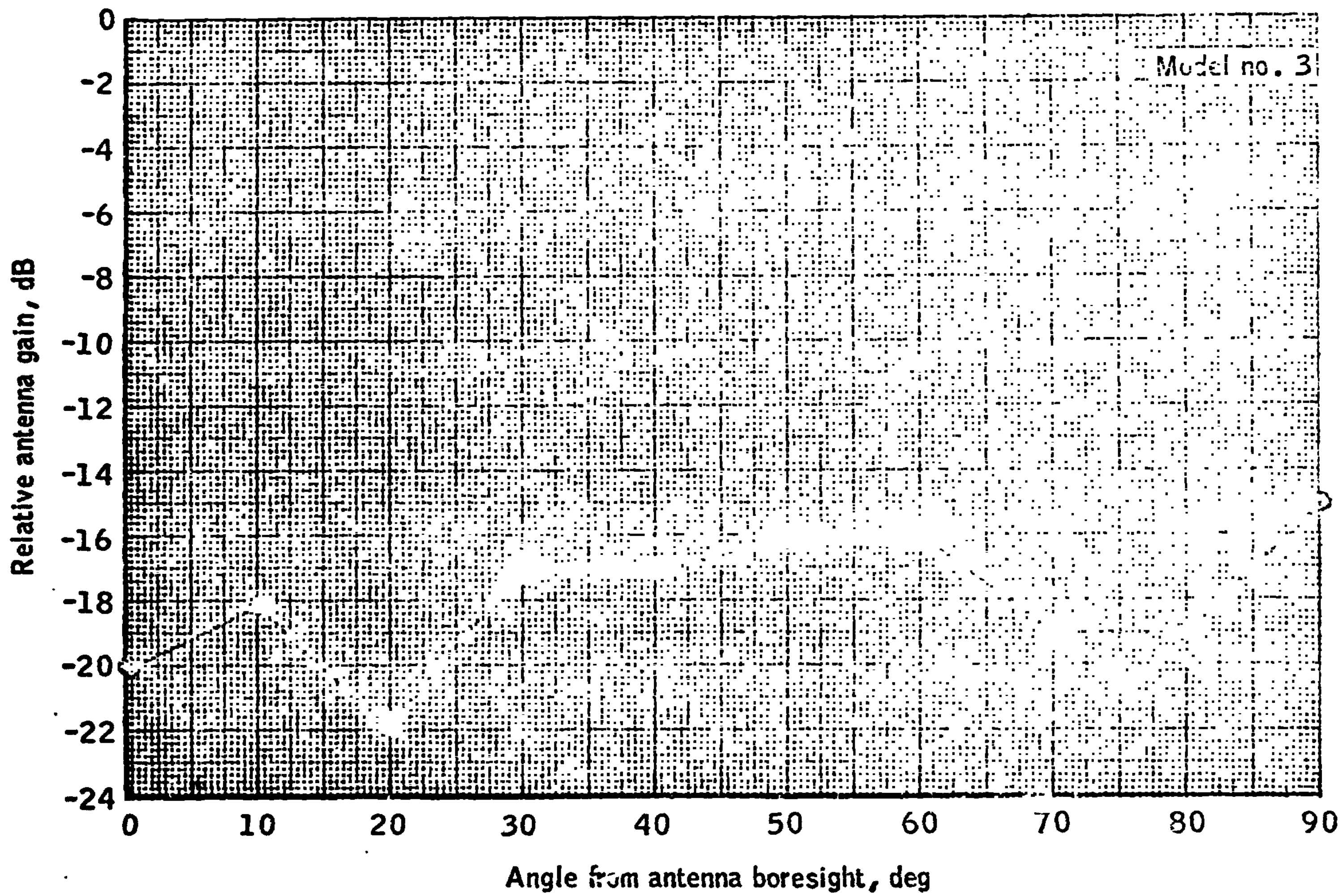

Figure 49.- Gain of CSM antenna covered by Model 3 after arc jet test with reference to uncovered CSM antenna versus the angle from the antenna boresight.

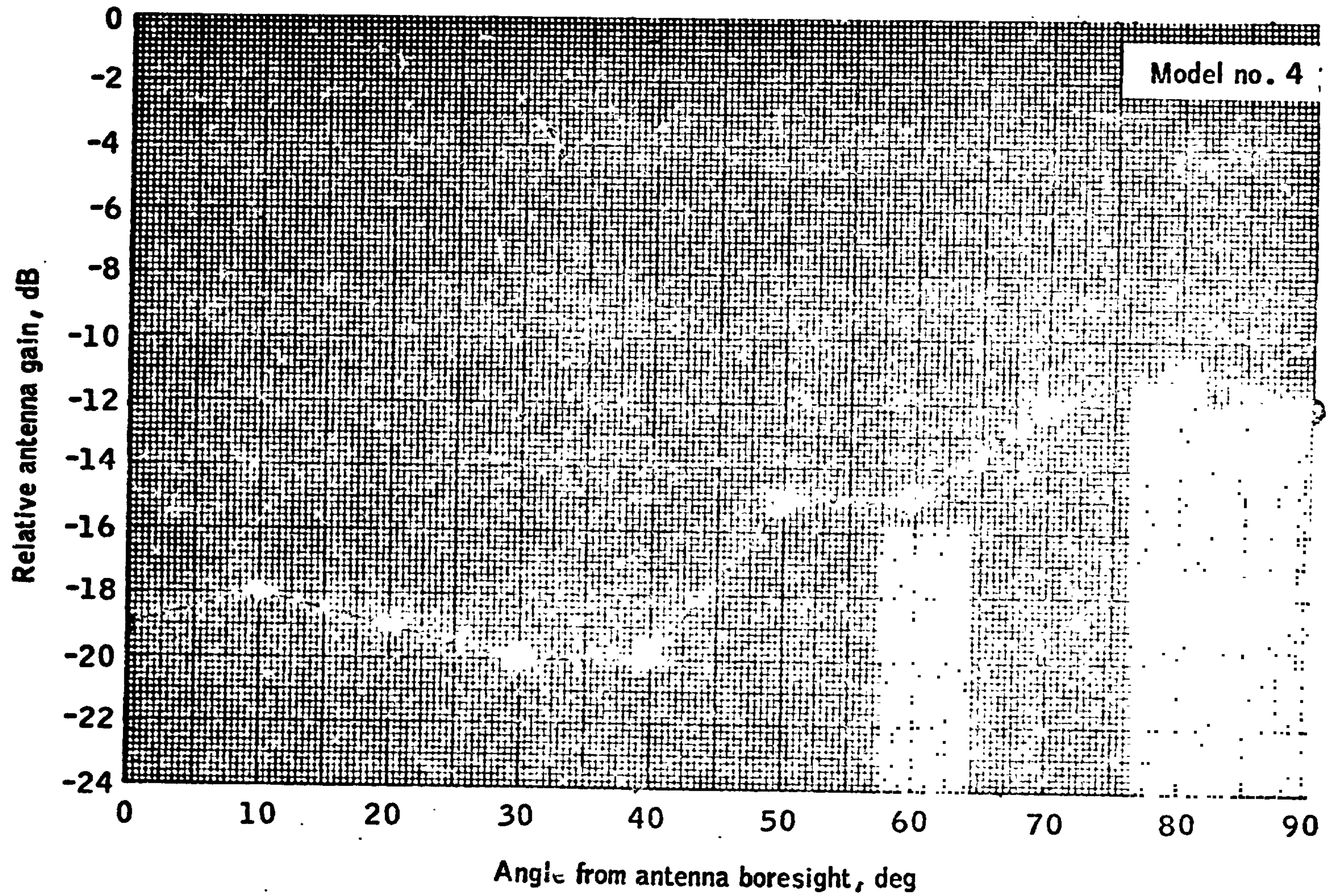

Figure 50.- Gain of CSM antenna covered by Model 4 after arc jet test with reference to uncovered CSM antenna versus the angle from the antenna boresight.

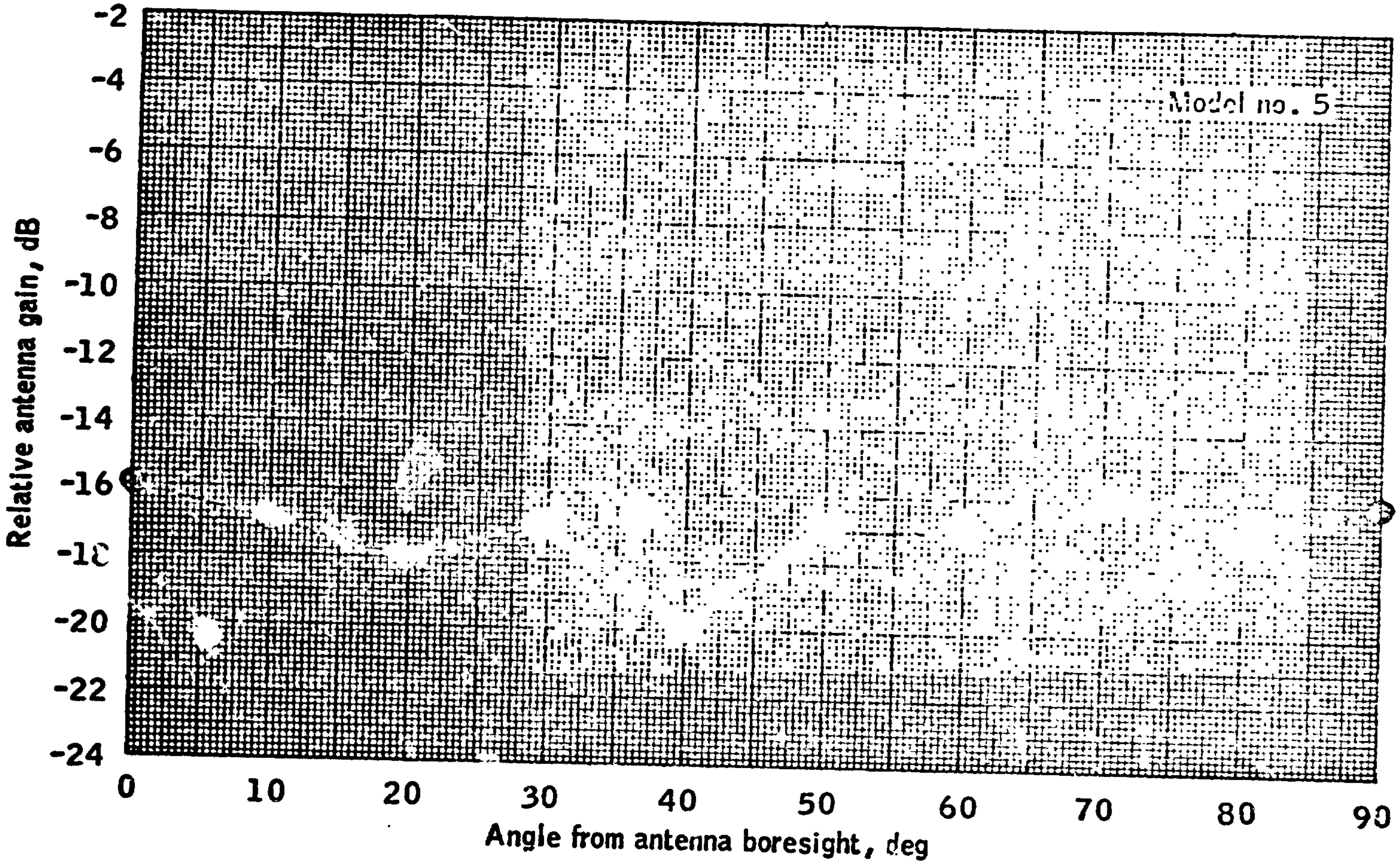

Figure 51.- Gain of CSM antenna covered by Model 5 after arc jet test with reference to uncovered CSM antenna versus the angle from the antenna boresight.

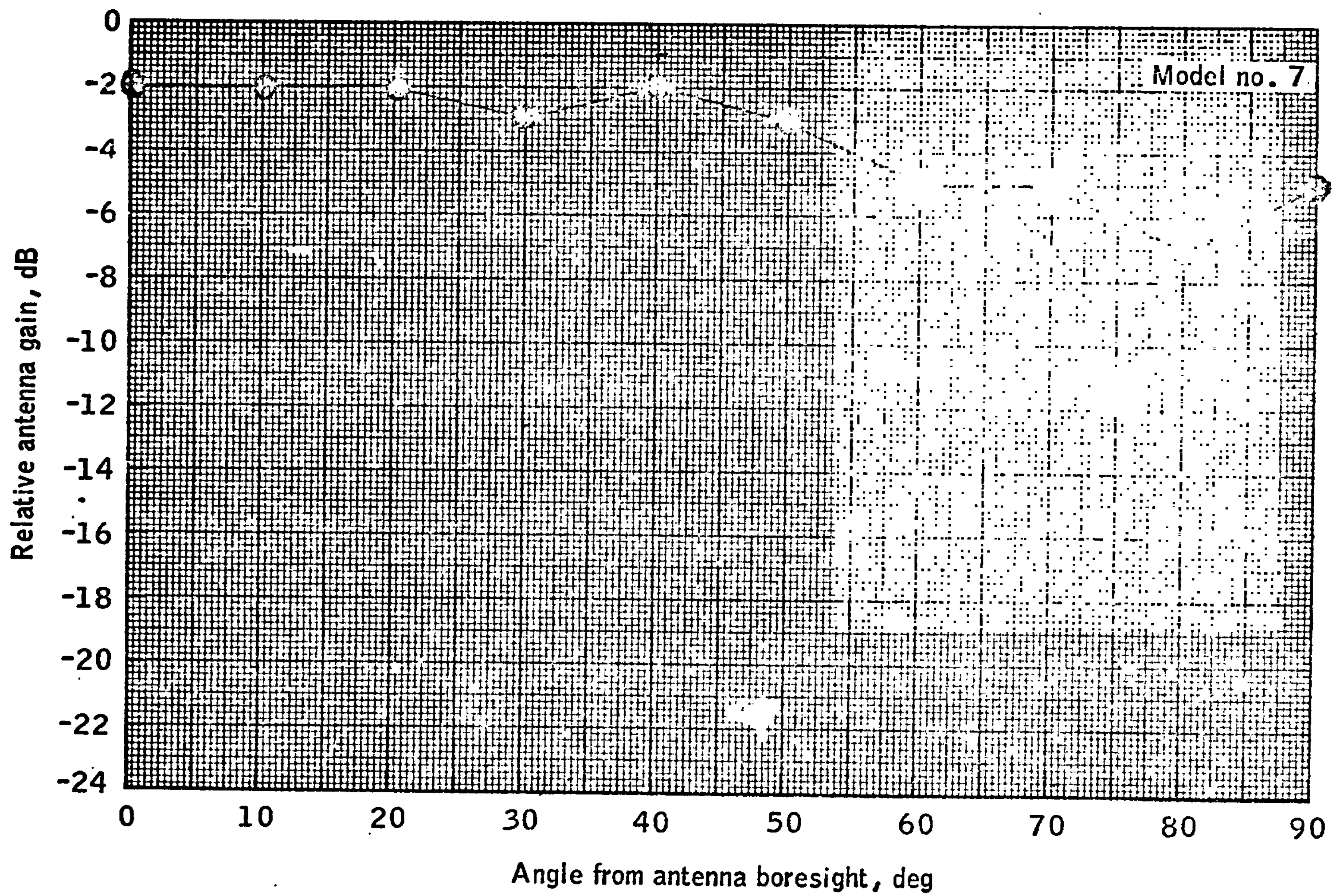

Figure 52.- Gain of CSM antenna covered by Model 7 after arc jet test with reference to uncovered CSM antenna versus the angle from the antenna boresight.

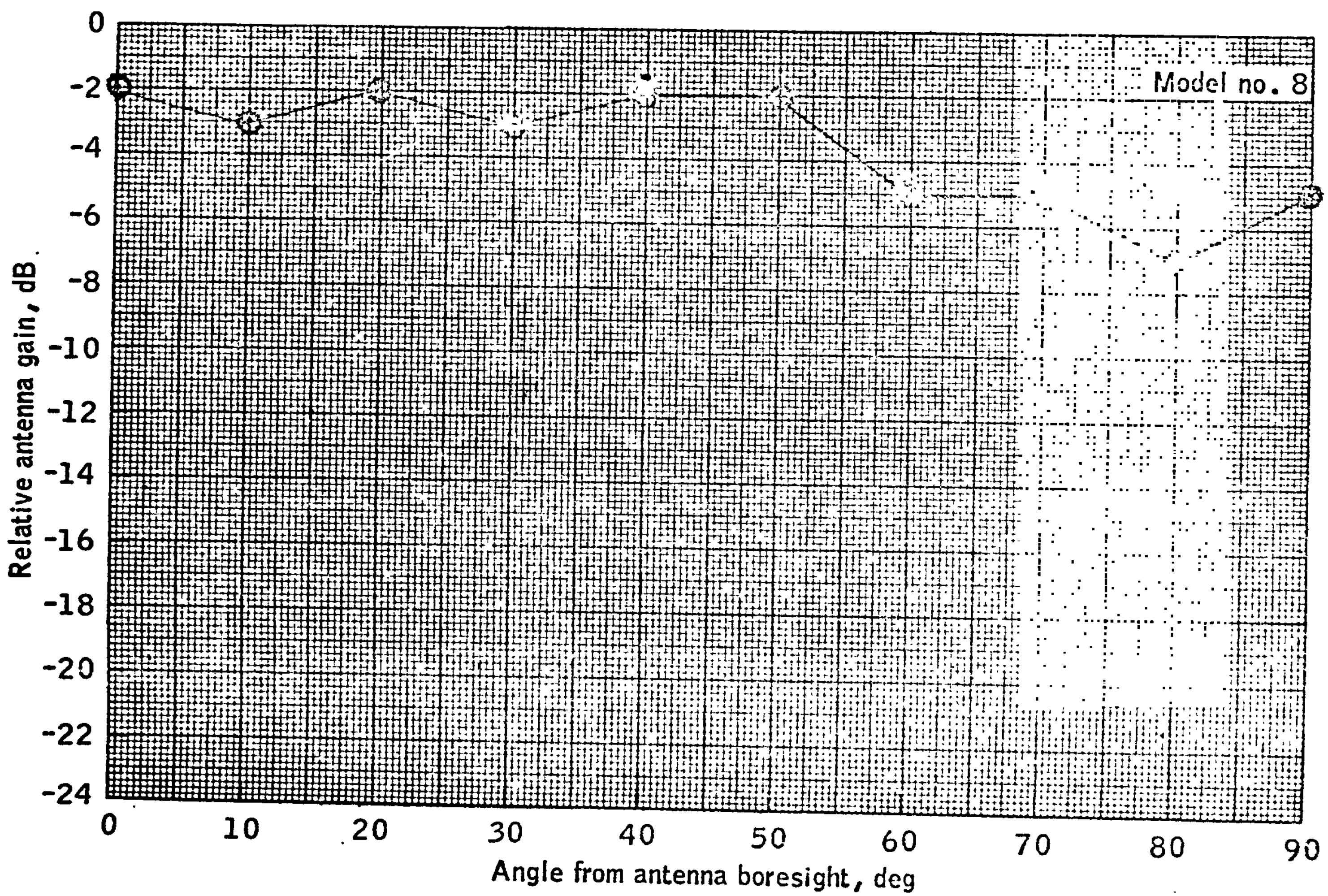

Figure 53.- Gain of CSM antenna covered by Model 8 after arc jet test with reference to uncovered CSM antenna versus the angle from the antenna boresight.

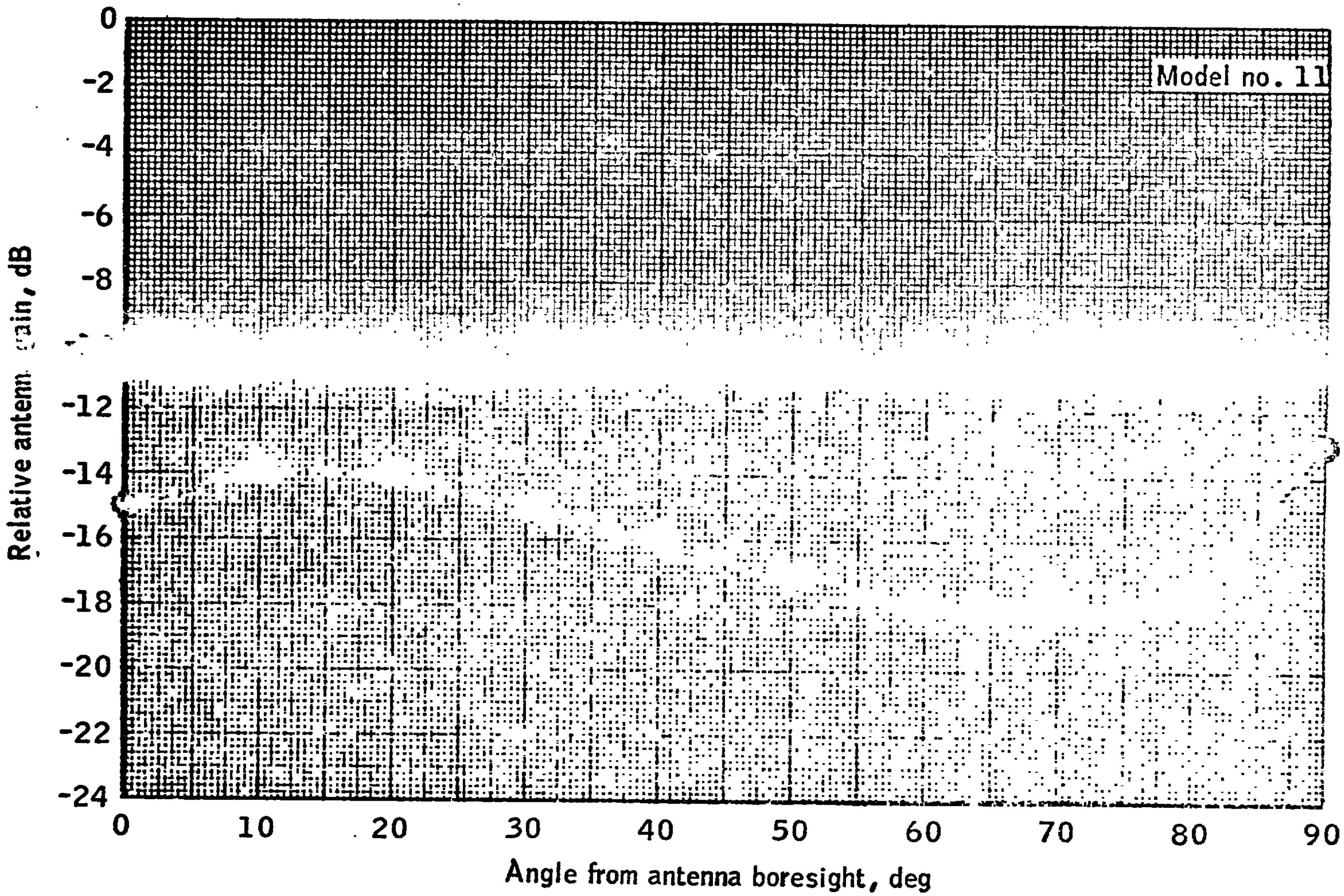

Figure 54.- Gain of CSM antenna covered by Model 11 after arc jet test with reference to uncovered CSM antenna versus the angle from the antenna boresight.

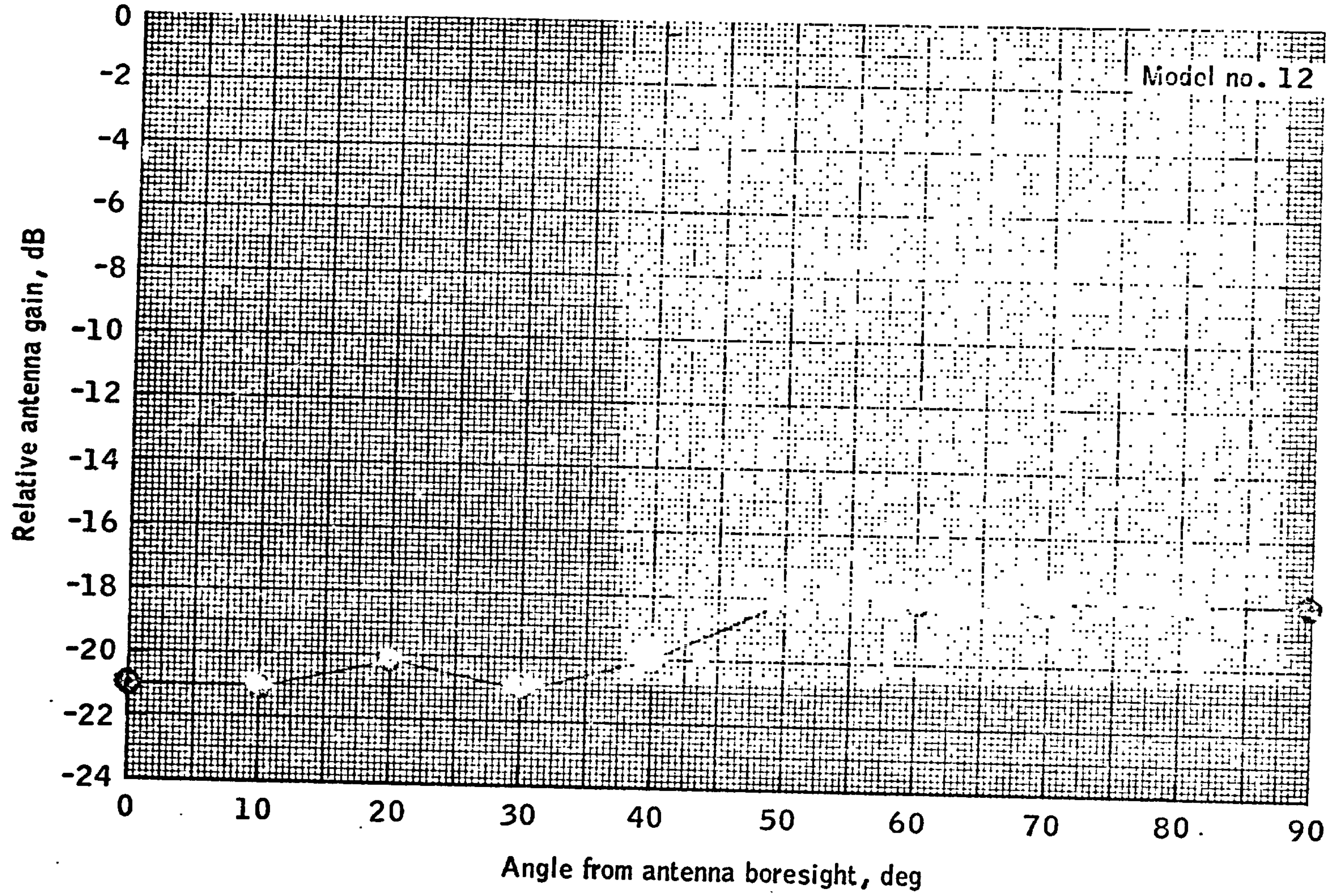

Figure 55.- Gain of CSM antenna covered by Model 12 after arc jet test with reference to uncovered CSM antenna versus the angle from the antenna boresight.

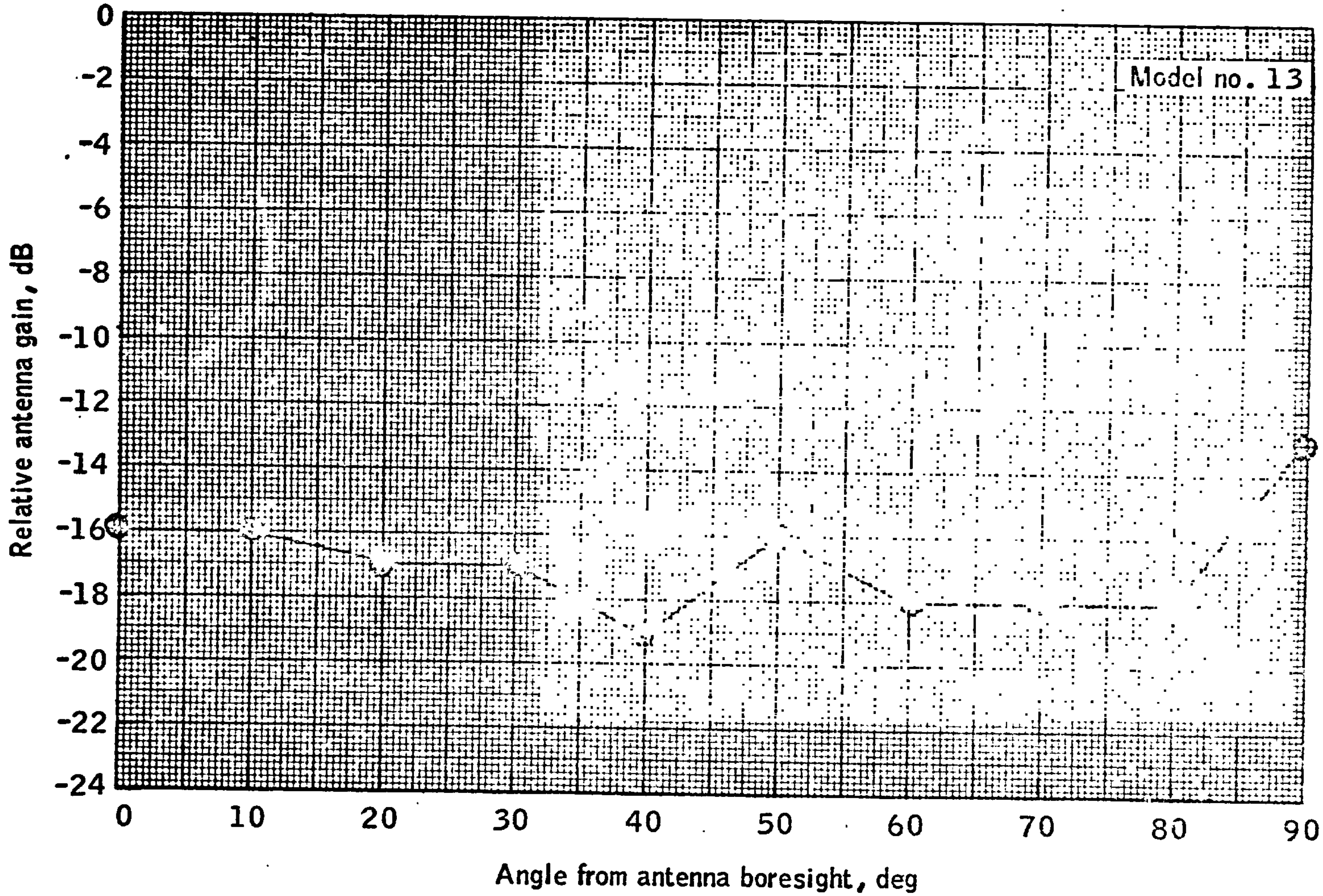

Figure 56.- Gain of CSM antenna covered by Model 13 after arc jet test with reference to uncovered CSM antenna versus the angle from the antenna boresight.

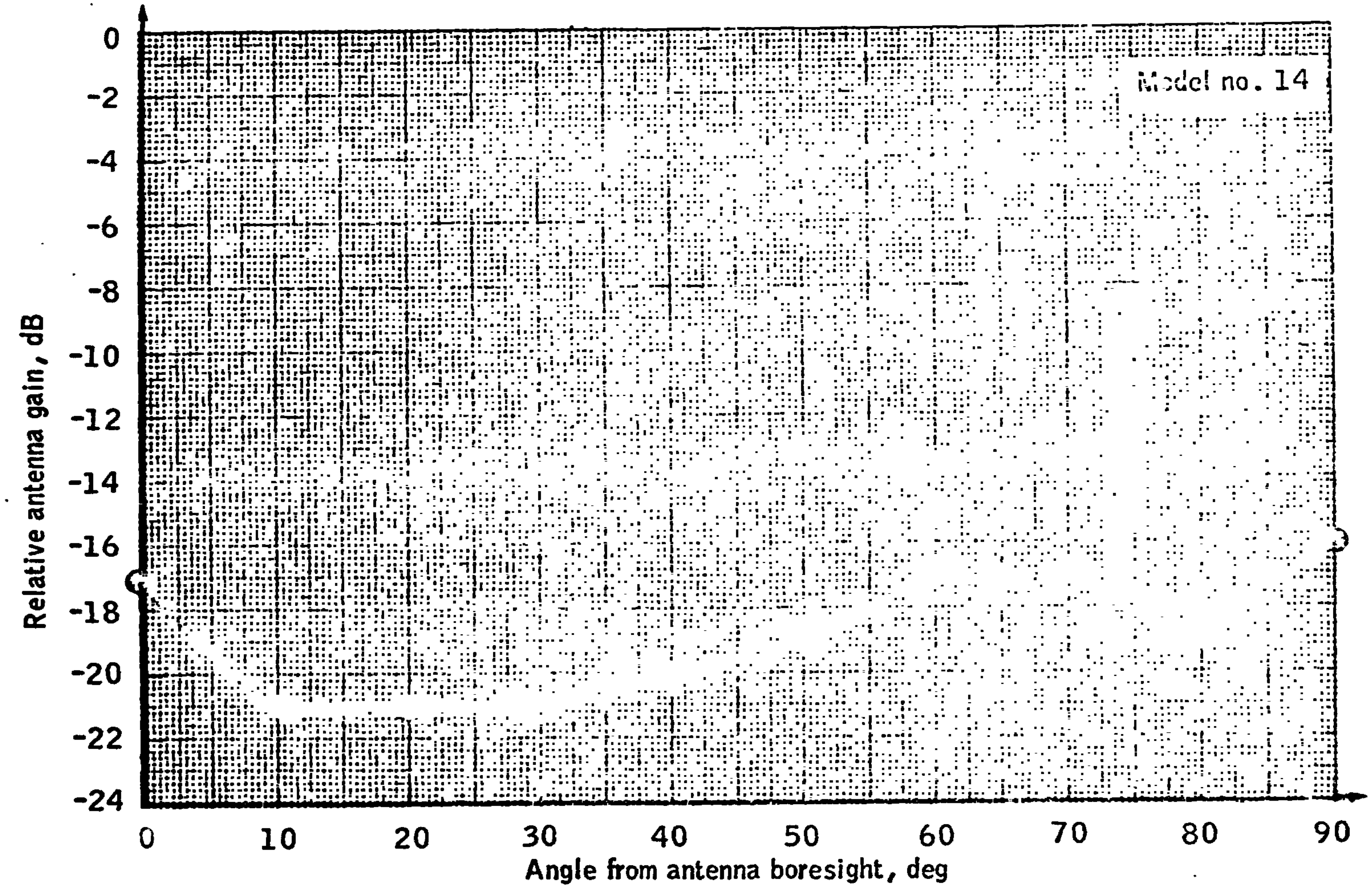

Figure 57.- Gain of CSM antenna covered by Model 14 after arc jet test with reference to uncovered CSM antenna versus the angle from the antenna boresight.

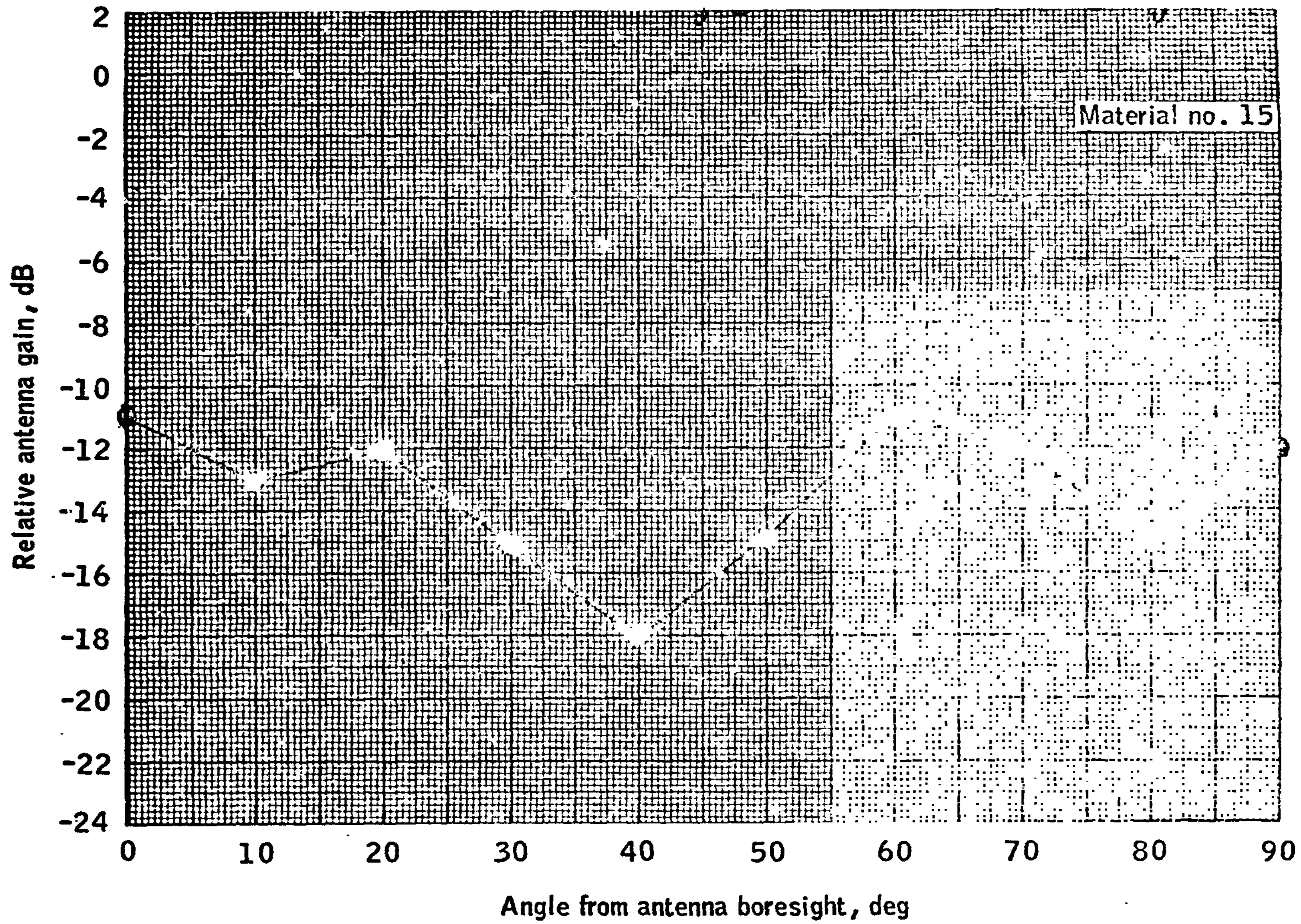

Figure 58.- Gain of CSM antenna covered by Model 15 after arc jet test with reference to uncovered CSM antenna versus the angle from the antenna boresight.

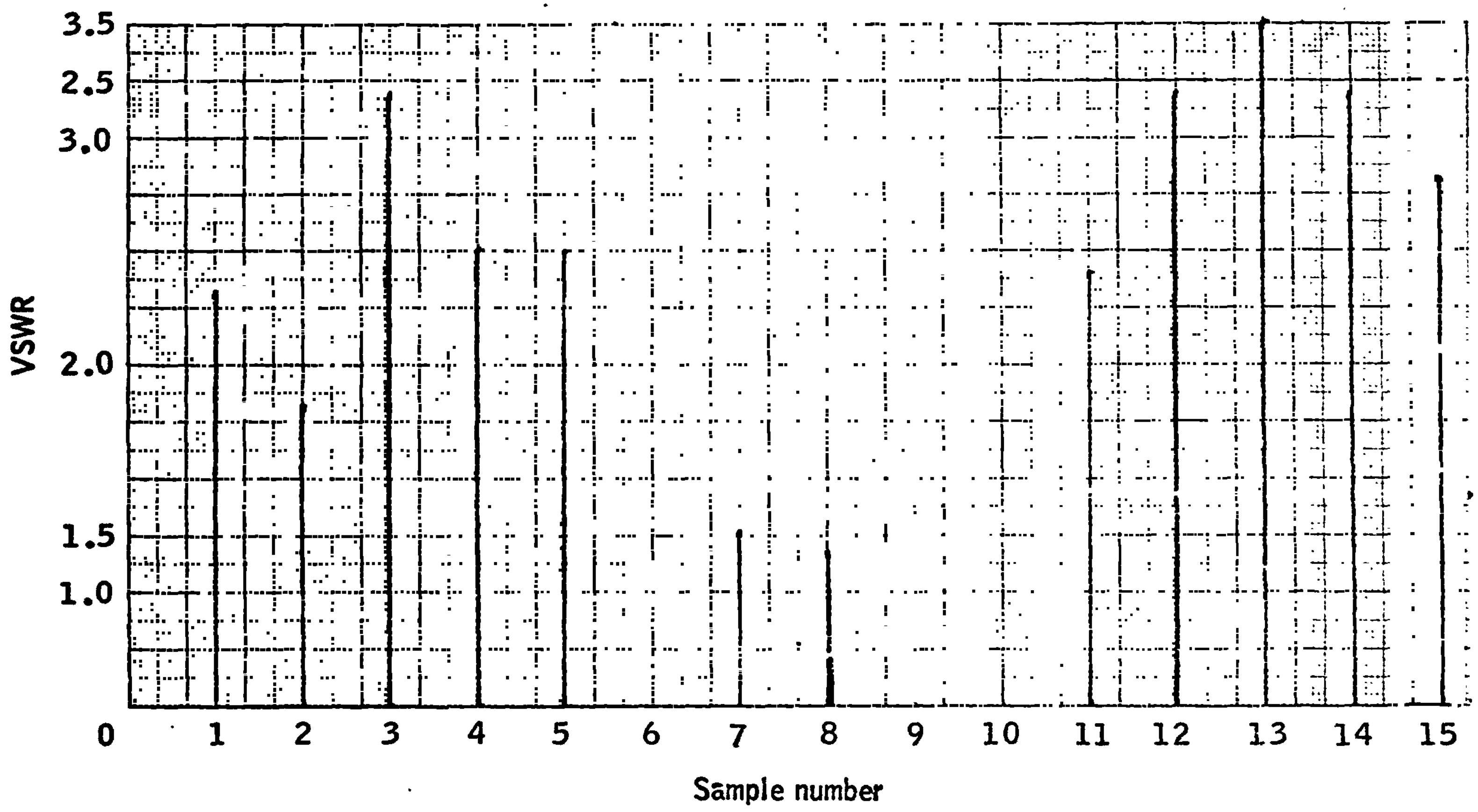

Figure 59.- VSWR of CSM antennas under charred covering material versus the sample number.

NASA — MSC